TITLE: Receptor-associated independent cAMP nanodomains (RAINs) mediate spatiotemporal specificity of GPCR signaling

AUTHORS:

Selma E. Anton[1,2,], Charlotte Kayser[1*], Isabella Maiellaro[2,3*], Katarina Nemec,[1,2], Jan Möller[1,2], Andreas Koschinski[4], Paolo Annibale[1], Manuela Zaccolo[4], Martin Falcke[1,5], Martin J. Lohse[1,2,6,7,8,9,#], and Andreas Bock[1,2,8,#]*

AFFILIATIONS:

[1]Max Delbrück Center for Molecular Medicine in the Helmholtz Association, Robert-Rössle-Straße 10, 13125 Berlin, Germany

[2]Institute of Pharmacology and Toxicology, University of Würzburg, Versbacher Str. 9, 97078 Würzburg, Germany

[3]School of Life Sciences, Department of Neuroscience, University of Nottingham, Nottingham NG7 2UH, UK

[4]Department of Physiology, Anatomy and Genetics, University of Oxford, Parks Road, OX1 3PT, Oxford, UK

[5]Department of Physics, Humboldt University, Newtonstr. 15, 12489 Berlin, Germany

[6]Institute for Chemistry and Biochemistry, Free University Berlin, Takustr. 3, 14195 Berlin, Germany

[7]ISAR Bioscience Institute, Semmelweisstraße 5, 82152 Munich/Planegg, Germany

[8]Senior author

[9]Lead Contact

*These authors contributed equally

#correspondence should be addressed to m.lohse@mdc-berlin.de or martin.lohse@isarbioscience.de and andreas.bock@mdc-berlin.de

Drs. Andreas Bock and Martin J. Lohse
Max Delbrück Center for Molecular Medicine in the Helmholtz Association
Robert-Rössle-Str. 10
13125 Berlin
Germany
Phone: +49 30 9406 1745

SUMMARY:

G protein-coupled receptors (GPCRs) are key physiological and therapeutic membrane proteins that relay extracellular stimuli into specific cellular functions. Cells express many different GPCRs, however, GPCRs signal to only a few second messengers such as cAMP, and it is therefore largely unknown how cells may distinguish between the signals triggered by different GPCRs in order to precisely orchestrate their complex functions.

Here we demonstrate the ability of individual GPCRs to signal via very small, localized signaling domains that are independent from those of other receptors. We show that low concentrations of glucagon-like peptide 1 (GLP-1), a key regulator of glucose metabolism, or isoproterenol, an agonist for β-adrenergic receptors, exclusively generate receptor-associated cAMP pools that do not equilibrate with other cellular cAMP compartments. Thus, the GLP-1 receptor cAMP compartment is protected from cAMP influx originating from stimulated β_2-adrenergic receptors. Using a set of novel FRET-based cAMP biosensors that are linked at defined distances from the GLP-1 receptor, we map the cAMP gradients that surround the receptors with tens of nanometer precision. We find that cAMP levels decrease at distances of tens of nanometers from the receptors, and this size also defines the area of cAMP signaling via protein kinase A, thereby constituting self-sufficient, receptor-associated, independent cAMP signaling nanodomain (RAINs). The existence of many such RAINs in a single cell allows cells to operate and process hundreds of independent cellular switches and signals at any one time, rather than function in a simple global "on/off" manner.

KEYWORDS:

G protein-coupled receptors, cAMP, compartmentation, cell signaling, FRET, biosensors, nanodomains, spatiotemporal signaling, diffusion, GLP-1

INTRODUCTION

Receptors and their downstream signaling pathways regulate essentially all functions of multicellular organisms. The main class of receptors is constituted by G protein-coupled receptors (GPCRs) and their downstream intracellular second messengers, notably cAMP and calcium (Rosenbaum et al., 2009; Weis and Kobilka, 2018). The human body expresses more than 800 GPCRs (Fredriksson et al., 2003; Hauser et al., 2017; Insel et al., 2015; Sriram and Insel, 2018), and approximately half of these sense extracellular ligands such as neurotransmitters and hormones, which modulate most physiological responses. More than 200 GPCRs regulate receptor-specific cell functions primarily through modulation of cAMP (Avet et al., 2020; Inoue et al., 2019; Pandy-Szekeres et al., 2018; Southan et al., 2016).

Since a single cell can express up to 100 different GPCRs (Insel et al., 2015), it poses a formidable challenge for a cell to distinguish between the inputs from its different GPCRs so that specific downstream cell functions would result. This appears particularly difficult for the many GPCRs that stimulate the intracellular concentration of cAMP, which is considered a highly diffusible molecule, which would, consequently, rapidly equilibrate across a cell and would, thus, produce the same biochemical response irrespective of the specific GPCR.

Attempts to search for specific signaling signatures of different GPCRs have been made for several decades. Thus, it has been shown long ago that in some cells, for example cardiac myocytes and hepatocytes, two different GPCRs may increase intracellular cAMP levels to the same extent, but that stimulation of these two GPCRs may have distinct effects on cell functions (Brunton et al., 1979; Buxton and Brunton, 1983; Di Benedetto et al., 2008; Hayes et al., 1979; Hayes et al., 1980; Nikolaev et al., 2010). A classic example is the observation that isoproterenol (via β-adrenergic receptors) and prostaglandin E_1 (via EP receptors) cause the same increase in cellular cAMP, but only isoproterenol increases contractile force of the heart and activates glycogen metabolism (Buxton and Brunton, 1983). Similarly, we have shown that

in cardiac myocytes stimulation of β_2-adrenergic receptors (β_2ARs) increases cAMP only locally, whereas stimulation of β_1ARs in the same cells increases cAMP globally, eventually leading to changes in gene transcription (Bathe-Peters et al., 2021; Bathe-Peters M, 2021; Nikolaev et al., 2006; Nikolaev et al., 2010). Another set of examples suggests that under basal conditions cAMP levels at the cell membrane may be higher than in the bulk cytosol and that low concentrations of agonists may be sufficient to trigger responses limited to the cell membrane (Agarwal et al., 2014; Civciristov et al., 2018; Halls and Cooper, 2010; Rich et al., 2000; Rich et al., 2001; Rich et al., 2007). Such studies have given rise to the concept that compartmentation of cAMP signaling may describe the ability of cells to spatially separate different cAMP signals and, consequently, to trigger distinct downstream responses (Langeberg and Scott, 2015; Lefkimmiatis and Zaccolo, 2014; Maiellaro et al., 2016; Scott and Pawson, 2009; Surdo et al., 2017; Taylor et al., 2012; Tovey et al., 2008; Wong and Scott, 2004).

For a long time, the concept of compartmentation appeared to be contradicted by observations that cAMP is an essentially freely diffusible second messenger (Agarwal et al., 2016; Bacskai et al., 1993; Chen et al., 1999; Huang and Gillette, 1993; Lohse et al., 2017; Nikolaev et al., 2004; Nikolaev et al., 2006; Richards et al., 2016), which would preclude the formation of intracellular concentration gradients and the formation of subcellular compartments. However, very recently we have shown that under basal conditions cAMP is mostly bound to intracellular binding sites, and that free diffusion only occurs once its levels are elevated well above the number of its binding sites (Bock et al., 2020). This is supported by the recent discovery of liquid-liquid phase separation of PKA-RIα that acts as a sponge to sequester cAMP (Zhang et al., 2020). We have further shown that this leads to very low concentrations of free cAMP, which in turn allows the cAMP phosphodiesterases to generate nanometer-size domains of even lower cAMP, in which local cAMP targets are protected from cellular cAMP signals (Bock et al., 2020).

Along these lines, we reasoned that the existence of cAMP binding sites at micromolar concentrations might provide a mechanism to generate and shape cAMP signals triggered by receptor stimulation and might permit the formation of gradients of elevated cAMP concentrations around individual GPCRs. Such spatially limited cAMP gradients might in turn enable cells to specifically 'sense' cAMP signals stemming from a particular GPCR, and to propagate GPCR-specific cAMP signals to defined downstream cell functions.

We therefore set out to search for such domains of high cAMP concentrations associated with GPCRs. To do so, we investigated specifically two types of G_s-coupled GPCRs: first, the glucagon-like peptide-1 receptor (GLP-1R), a receptor playing a key role in glucose metabolism and a major target in diabetes therapy (Drucker, 2018; Drucker et al., 2017) that responds to peptidic as well as non-peptidic agonists (Fletcher et al., 2016; Muller et al., 2019; Zhao et al., 2020). GLP-1Rs regulate insulin secretion in pancreatic β-cells via cAMP-dependent stimulation of PKA, and this effect appears to require cellular compartmentation of PKA via anchoring proteins (Lester et al., 1997). In addition, we studied the β_2-adrenergic receptor, the major receptor mediating the effects of epinephrine and norepinephrine, which – as outlined above – has also been linked to compartment-dependent downstream effects (Buxton and Brunton, 1983; Nikolaev et al., 2006; Nikolaev et al., 2010).

Here, we aimed to explore such domains by fusing a FRET-based cAMP biosensor to receptors with ruler-like spacers of defined nanometer length, in order to obtain maps of cAMP levels at defined distances from the receptors. To finally show the relevance of such putative domains of high cAMP, we measured activation of downstream PKA with similarly targeted constructs that permit the generation of activity maps around individual GPCRs.

RESULTS:

To provide direct evidence for the existence of putative cAMP compartments in the vicinity of individual GPCRs, we designed and used three different FRET-based cAMP biosensors. The first is the novel FRET-based biosensor *GLP1R-camps* that is composed of the human glucagon-like peptide-1 receptor (GLP-1R) fused to the cAMP biosensor *Epac1-camps* (Nikolaev et al., 2004*)* (**Figure 1**) and that allows measuring cAMP in the immediate vicinity of the GLP-1R. We further used a second novel cAMP biosensor, *Epac1-camps-CAAX*, to measure cAMP in the immediate vicinity of the cell membrane, and, finally, untargeted *Epac1-camps* serving as a sensor for ubiquitous cytosolic cAMP levels (**Figure 1A**).

The functionality and correct expression of the new sensors was assessed in several control experiments (**Figures 1A, S1**). These experiments showed that the sensors retained the functionalities of their parent components by demonstrating that (a) the *GLP1R-camps* sensor binds GLP-1-(7-36)-amide (from here on termed GLP-1) and stimulates whole-cell cAMP production with nanomolar potency similar to wild-type GLP-1 receptors (**Figure S1A**), (b) upon stimulation with GLP-1, single HEK cells transiently expressing *GLP1R-camps* responded with a change in FRET ratio (**Figure S1B**), (c) this FRET change was specifically indicating increases in cAMP, since a mutated construct *GLP1R-camps-R279E*, which does not bind cAMP, showed no FRET change upon addition of a variety cAMP-increasing stimuli (**Figure S1C**), and (d) all three sensors (*GLP1R-camps, Epac1-camps-CAAX, and Epac1-camps)* had the same affinity for cAMP (**Figure S1D**). Finally, we confirmed that the three sensors displayed the expected subcellular distribution when expressed in HEK cells: confocal microscopy showed that *GLP1R-camps* and *Epac1-camps-CAAX* were expressed at the cell membrane while untargeted *Epac1-camps* showed a ubiquitous cytosolic expression (**Figure 1A**).

To assess basal cAMP concentrations in the vicinity of the GLP-1R as well as the compartments surveyed by the other sensors, we employed a previously developed calibration approach for cAMP determination in intact cells (Borner et al., 2011) (**Figure 1B**). This approach uses inhibition of basal activity of adenylyl cyclase with MDL-12,330A in order to reach minimal, basal levels of cAMP (**Figure 1B**; R_{MIN}). Addition of 100 µM of MDL-12,330A to cells expressing either of the three sensors resulted in quite distinct FRET responses: it strongly decreased cAMP levels at the GLP-1R and at the cell membrane in general (**Figure 1C**, orange and green traces, respectively), but much less in the bulk cytosol (**Figure 1C**, blue trace).

Saturation of all sensors was subsequently reached by application of the cell-permeable, specific Epac-activator 8-Br-2'-O-Me-cAMP-AM, followed by inhibition of endogenous phosphodiesterases (PDEs) with IBMX, yielding FRET-values for maximal cAMP signals (**Figures 1B, C**; R_{MAX}). Calculation of relative basal cAMP levels from appropriate calibration curves (Borner et al., 2011) revealed that these levels were similar in the vicinity of GLP-1 receptors and in the cell membrane compartment (**Figure 1D**, and compare initial values in **Figure 1C**), which is expected considering that *GLP1R-camps* is exclusively membrane-localized. Interestingly, the levels appeared to be much lower for the cytosolic sensor *Epac1-camps* (**Figure 1D**). These data indicate that different basal cAMP concentrations may exist in different regions of a cell, with higher concentrations near the cell membrane than in bulk cytosol, confirming earlier notions of such differences (Agarwal et al., 2014; Rich et al., 2000; Rich et al., 2001; Rich et al., 2007).

Low-concentrations of GLP-1 exclusively generate a GLP-1R-associated cAMP pool

To assess the cAMP dynamics in the different compartments, we stimulated HEK cells expressing either of the three sensors with various concentrations of GLP-1 and monitored the resulting changes in FRET (**Figure 2**). Upon stimulation with GLP-1, single HEK cells transiently expressing *GLP1R-camps* responded with a change in FRET ratio (**Figure 2B-D**).

Interestingly, low GLP-1 (1 pM) – a concentration which hardly increased global cellular cAMP levels (**Figure S1A**) – led to a robust increase in cAMP levels in the direct vicinity of GLP-1R (**Figure 2B**, orange). In contrast, 1 pM GLP-1 induced a significantly smaller increase in cAMP at the cell membrane (**Figure 2B**, green), and – in line with whole-cell cAMP data (**Figure S1A**) – showed virtually no cAMP increase in the cell cytosol (**Figure 2B**, blue). As all three sensors (*GLP1R-camps, Epac1-camps-CAAX, and Epac1-camps)* display the same affinity for cAMP (**Figure S1D**) and are expressed at similar expression levels (**Figure S2D**), these data demonstrate that low concentrations of GLP-1 produce a local cAMP pool which appears to be confined to the immediate vicinity of GLP-1 receptors and spatially distinct from other compartments of the cell. In addition, kinetic analysis indicated that cAMP concentrations increase faster directly at GLP-1 receptors than in the cell cytosol (**Figure S2**).

Elevated GLP-1 concentrations (1 nM and 100 nM) saturated cAMP levels at the GLP-1R, the cell membrane and in the cytosol and thereby abolished these cAMP gradients (**Figure 2C, D**).

The GLP-1R-associated cAMP pool is protected from a foreign GPCR stimulus

Our experiments show that stimulation of *GLP1R-camps* with its cognate agonist GLP-1 produces a receptor-associated cAMP pool which, at low agonist concentrations, does not appear to spread to other cellular compartments on the timescale of our measurements (i.e. minutes) (**Figure 2B-D**). Thus, cAMP that is produced *inside* this receptor-associated compartment is severely hindered in its ability to diffuse *outside* of this compartment. We hypothesized that, reciprocally, cAMP from *outside* sources might be restricted in its ability to diffuse *into* the GLP-1 receptor-associated compartment. To provide experimental evidence for this hypothesis, we stimulated endogenous β_2-adrenergic receptors (β_2-ARs) with the synthetic agonist isoproterenol (Iso) and measured increases in cAMP within the GLP-1R-associated compartment using *GLP1R-camps* as the sensor (**Figure 2E-G**). As a reference for cAMP

proximal to the cell membrane, we used again *Epac1-camps-CAAX* as the sensor, and untethered *Epac1-camps* to determine bulk cytosolic cAMP.

Stimulation of β_2-ARs with low concentrations of Iso (10 pM) strongly increased cAMP levels at the cell membrane; however, the cAMP levels in the GLP-1R-associated compartment were significantly lower, and cytosolic cAMP remained unchanged (**Figure 2E**). Addition of 100 pM Iso caused a large cAMP response both at the cell membrane and in the cytosol. Interestingly, however, the resulting increase in cAMP levels in the GLP-1R-associated compartment remained significantly lower (**Figure 2F**). Higher Iso concentrations (10 nM) led to the same relative cAMP increase in all three compartments and thus dissipated the observed cAMP gradients (**Figure 2G**). Our data suggest that, similar to GLP-1Rs, stimulation of β_2-ARs produced at least three spatially segregated pools of cAMP. However, and in stark contrast to GLP-1R stimulation, the order in which these compartments show increases in cAMP is different: first, the cAMP levels close to the cell membrane increase, then cAMP levels inside the GLP-1R-associated compartment, followed by the cell cytosol. These findings contrast with those measured upon GLP-1R stimulation, where we observed first an increase within the GLP-1R-associated compartment, then the cell membrane compartment, and finally the cytosol (**Figure 2B-D**).

Together, these data strongly argue for the existence of distinct receptor-associated cAMP pools within a single cell which are spatially segregated and under the control of individual GPCRs. Stimulation of a given receptor would thereby increase cAMP initially in its own immediate compartment (and not affect the compartments of other receptors), followed by the cell membrane compartment and finally the cytosol. Importantly, at low GLP-1 concentrations, cAMP gradients are stationary and cAMP levels between different compartments do not equilibrate.

Optical mapping of GLP-1R-associated cAMP pools reveals nanometer size domains

We hypothesized that the size of receptor-associated compartments needs to be very small in order for a cell to organize signaling inputs from many GPCRs simultaneously with sufficient spatial separation. To provide direct values for the size of such compartments in intact cells, we set out to precisely map the dimensions of these receptor-associated cAMP compartments. To do so, we developed a set of novel tools where the *Epac1-camps* sensor is placed at defined distances from the GLP-1R. To achieve these defined distances, we used genetically-encodable single-alpha-helical domain (SAH) linkers based on ER/K repeats (Bock et al., 2020; Sivaramakrishnan and Spudich, 2011). SAH linkers have been shown to have a size of nanometers and a rod-like shape which allows to position two proteins at defined distances from each other.

Based on such linkers we generated *"GPCR-nanorulers"* by placing a 30 nm SAH domain linker (SAH30) derived from a Kelch-motif family protein from *Trichomonas vaginalis*, or a tandem spacer of two such domains, between the GLP-1R and *Epac1-camps* to create *GLP1R-SAH30-camps* or *GLP1R-SAH60-camps*, respectively (**Table S1**). These constructs should, therefore, measure cAMP levels at 30 nm or 60 nm distance from the receptor in real-time and in intact cells. To verify that the SAH linkers did indeed result in the predicted spacing, we generated a reference construct, which was a membrane-localized version of SAH60 sandwiched between two HaloTags fluorescently labeled with Halo JF-646 (**Figure S3A**). We then performed direct stochastic optical reconstruction microscopy (dSTORM) in fixed cells expressing the labeled construct to measure the distance between the two labels and, thereby, the length of the SAH60 linker (**Figures 3A, S3**). Analysis of the frequency distribution demonstrated that the most abundant molecules had a length of 60 nm (peak of distribution at 69 nm) (**Figures S3B, C**), and, consequently, confirmed that an individual SAH30 linker has a length of approximately 30 nm. Moreover, we confirmed that the GPCR-nanorulers were expressed at similar expression levels (**Figure S3D**), had the same potency for stimulating

cAMP production as GLP-1 wild-type receptors (**Figure S3E**), and had the same affinity for cAMP as *Epac1-camps* (**Figure S3F**).

Stimulation of HEK cells with 1 pM GLP-1 – a concentration that robustly increased cAMP within the GLP-1R-associated compartment but virtually not in the cell cytosol (**Figure 2**) – led to a significantly smaller relative FRET change in cells expressing *GLP1R-SAH30-camps* compared to *GLP1R-camps* (**Figure 3B**). As the affinities of the two sensors for cAMP are equal (**Figure S3F**), these data demonstrate that the cAMP levels at 30 nm distance from the receptor are significantly lower than in the direct vicinity of the receptor (**Figure 3B,E**). However, the cAMP concentrations measured with *GLP1R-SAH30-camps* were significantly higher than in the cell cytosol (**Figure 3B,E**), suggesting that the GLP-1R-associated cAMP compartment has a dimension of more than 30 nm.

To measure cAMP beyond the 30 nm distance, we stimulated also HEK cells expressing the longer *GLP1R-SAH60-camps* nanoruler with 1 pM GLP-1. This resulted in significantly smaller relative FRET changes than were seen with *GLP1R-SAH30-camps* and *GLP1R-camps* (**Figure 3B, E**), and which were only slightly, albeit significantly, larger than the signals measured in the cell cytosol (**Figure 3B, E**), suggesting that the GLP-1R-associated cAMP pool has a diameter of approximately 60 nm. Given the dimensions of these receptor-associated cAMP pools we propose to define them as *receptor-associated independent cAMP nanodomains (RAINs)*.

To assess how these domains change upon stronger stimulation of the receptors, we performed similar experiments with 1 nM GLP-1 (**Figure 3C**). Interestingly, at these higher concentrations, differences in FRET ratios at 0, 30 and 60 nm distance from the receptor were no longer visible, indicating that the concentration gradients seen with 1 pM GLP-1 were abolished (**Figure 3C, F**).

As the GLP-1R-associated nanodomains are protected from cAMP generated by β_2-ARs (**Figure 2E**), we wondered whether the *GLP1R-nanorulers*, i.e. *GLP1R-SAH60-camps* and

GLP1R-SAH30-camps, would sense this 'foreign' cAMP earlier than *GLP1R-camps*. To test this hypothesis, we expressed all three constructs at similar levels and stimulated endogenous β_2-AR in HEK cells with 10 pM Iso (**Figure 3D**). In line with our hypothesis, *GLP1R-SAH60-camps* detected a significantly larger cAMP increase than *GLP1R-SAH30-camps* and *GLP1R-camps* (**Figure 3D, G**). These data demonstrate that GLP1R cAMP nanodomains are gradually protected from cAMP generated by different sources and, thus, further support the existence and shape of RAINs.

Localized PDE activity shapes the size of GLP-1R-associated cAMP nanodomains

PDEs have repeatedly been suggested to contribute to compartmentation of cAMP (Baillie, 2009; Baillie et al., 2019; Bender and Beavo, 2006; Fischmeister et al., 2006; Houslay, 2010; Stangherlin and Zaccolo, 2012). We have demonstrated recently that this is due to the fact that under basal physiological conditions, most cAMP is not freely diffusible but bound to specific sites, which results in free cAMP low enough that individual PDEs can shape cAMP concentration gradients (Bock et al., 2020). Therefore, we tested whether endogenous PDEs might have a role in shaping receptor-associated cAMP nanodomains. Pretreatment with the global PDE inhibitor IBMX (100 μM) by itself led to different FRET changes in direct vicinity of the GLP-1R and at 30 and 60 nm distances from the receptors. This suggests that PDE activity is different at certain nanometer distances from the receptor (**Figures 4A, B**). Interestingly, IBMX pretreatment abolished the differences in cAMP levels measured in the direct vicinity of vs. at 30 nm distance from the GLP-1 receptor upon stimulation with 1 pM GLP-1 (**Figure 4C**). These data suggest that localized PDE activity is a key factor in shaping the size of the receptor-associated cAMP nanodomain.

GLP-1 receptor nanodomain signaling requires tethered PKA

The observations that cAMP levels are higher in the immediate vicinity of a GPCR and that these domains are somewhat protected from the influx of cAMP generated at other receptors can only be explained if cAMP is not freely diffusible at these sites. We have recently discovered that cytosolic cAMP under basal conditions is buffered by binding to specific binding proteins, such as protein kinase A (PKA) (Bock et al., 2020). To assess whether similar mechanisms might account for the formation of cAMP gradients around GPCRs, we investigated whether local cAMP buffering sites exist within these receptor-associated cAMP nanodomains. We used the FRET-based PKA activity reporter *AKAR4* (Depry et al., 2011), which reports on endogenous PKA activity upon phosphorylation of its intrinsic PKA substrate. By fusing *AKAR4* to the C-terminus of the GLP-1R we generated the sensor (*GLP1R-AKAR4*) to test for endogenous PKA activity inside the receptor-associated cAMP nanodomain (**Figure 5A**). We confirmed that *GLP1R-AKAR4* stimulated cAMP production as efficiently as GLP-1 wild-type receptors and that *AKAR4* sensed PKA phosphorylation equally well independent of being tethered to GLP-1R (*GLP1R-AKAR*) or expressed in the cytosol (**Figure S4A, B**). Moreover, confocal microscopy of cells expressing *GLP1R-AKAR4* confirmed that it was appropriately localized at the cell membrane (**Figure 5A**, left lower panel). As a control for whole-cell PKA activity we expressed separately but stoichiometrically GLP-1R and *AKAR4*, which lead to whole-cell expression of *AKAR4* (**Figure 5A**, right lower panel).

Stimulation with 1 pM GLP-1 – the concentration that had increased cAMP within the GLP-1R-associated compartment but virtually not in the cell cytosol (**Figure 2**) – led to a strong, almost saturating increase in FRET ratio of the *GLP1R-AKAR4* sensor*,* indicating strong PKA activity inside the receptor-associated cAMP nanodomain (**Figure 5B**, orange trace). In contrast, the same GLP-1 concentration promoted only very little PKA activity in the cytosol as revealed by the non-fused *AKAR4* sensor (**Figure 5B**, blue trace). As before, no such differences were visible at higher GLP-1 concentrations (1 nM); under these conditions, PKA

was fully activated both in the receptor-associated cAMP nanodomain and in the cytosol (**Figure 5C**).

PKA is tethered to molecular signaling complexes by A-kinase-anchoring proteins (AKAPs) (Langeberg and Scott, 2015; Scott and Pawson, 2009; Taylor et al., 2012; Wong and Scott, 2004). This provides a means for cells to localize PKA activity to defined macromolecular signaling complexes at specific cellular locations, thereby exerting spatial control over PKA activity. Strikingly, when HEK cells expressing *GLP1R-AKAR4* were pretreated with St-Ht31, a peptide that disrupts protein-protein interactions between regulatory subunits of PKA and AKAPs, PKA activity in the receptor-associated cAMP nanodomain was entirely lost even upon stimulation with 1 nM GLP-1 (**Figure 5D**). Remarkably, disrupting AKAP/PKA interactions had no effect on cytosolic PKA activity under the same stimulation conditions (**Figure 5D**). As expected, pretreatment with the respective inactive control peptide St-Ht31-P had no effect on PKA activity inside the receptor-associated cAMP nanodomain (**Figure 5E**). These data unequivocally demonstrate the presence of localized PKA activity tethered to the GLP-1R-associated cAMP nanodomain. This local signaling complex constitutes a self-sufficient, independent signaling unit, in which local generation of cAMP by GLP-1 is directly translated into local PKA activity. Of note, since disruption of PKA tethering completely abolished GLP-1R nanodomain signaling, it is necessary that PKA molecules have to be located *inside* the GLP-1R nanodomain. This indicates that diffusion of other PKA molecules primarily located *outside* of the GLP-1R nanodomain into these domains does not occur or, at least, does not promote phosphorylation of PKA substrates tethered to the GLP-1 receptor.

Low-concentrations of isoproterenol generate a β_2-AR-associated cAMP pool

To test whether the existence of RAINs might be a general phenomenon, we aimed to demonstrate them also for another G_s-coupled receptor, the prototypical β_2-AR. We have shown above that β_2-AR-mediated cAMP stimulation leads to significantly higher cAMP increases at

the cell membrane than in the direct vicinity of GLP-1 receptors (**Figure 2E**). Furthermore, we have demonstrated that GLP-1Rs are protected in a gradual manner from cAMP generated by β_2-AR activation (**Figure 3D, 3G**). These data suggest that β_2-ARs may, in analogy to GLP-1Rs, also generate cAMP nanodomains.

To provide direct evidence for RAINs at β_2-AR, we designed and cloned *β_2AR-camps*, a biosensor consisting of the human wild-type β_2-AR fused to *Epac1-camps* (**Figure 6**). *β_2AR-camps* functions as wild-type β_2-AR with respect to cAMP production (**Figure S5A**) and shows correct membrane localization (**Figure 6B**). Stimulation of HEK cells that expressed *β_2AR-camps* or a bicistronic plasmid encoding β_2-AR and *Epac1-camps-CAAX* or *Epac1-camps* (for membrane or cytosolic cAMP detection, respectively) at similar expression levels (**Figure S5B**), with very low concentrations of Iso (1 pM) led to significantly larger cAMP increases at the β_2-AR and at the cell membrane than in the cytosol (**Figures 6C**). In contrast to GLP-1Rs, we did not observe differences in the cAMP levels at the β_2-AR and the cell membrane in HEK cells that express β_2-AR endogenously (albeit at much lower levels) (**Figure 6C**). In line with the data at GLP-1Rs, higher concentrations of Iso (10 pM) abolished β_2-AR cAMP nanodomains (**Figures 6D**).

Taken together, these data demonstrate that also β_2-AR form RAINs, which suggests that RAINs may be a general phenomenon of GPCRs.

Quantitative aspects of receptor-associated independent cAMP signaling nanodomains (RAINs)

We have shown that GPCRs generate receptor-associated cAMP nanodomains that stretch over several tens of nanometers and are protected from cAMP influxes produced by different GPCRs. The differences in cAMP concentrations in different compartments (receptor, cell membrane, cytosol, c. f. **Figure 2**) and at nanometer-distances from the receptor at steady-state (**Figure 4B**) are remarkable. We were wondering how these cAMP concentration profiles could be described in quantitative terms.

In the absence of any mechanism that restricts cAMP diffusion dynamics, the cAMP concentration profiles would be dictated by free diffusion and, thus, of hyperbolic nature. At low agonist occupancies (i.e. 1 pM GLP-1) one can assume that the distance between individual, ligand-bound receptors is much larger than the radius of the receptor-associated cAMP nanodomain, and, thus, at 1 pM GLP-1 stimulation we consider isolated cAMP concentration profiles under the control of single active GLP-1R's (**Methods S1**, for graphical illustration see **Figure 7A**). Assuming a constant cAMP diffusion coefficient within RAINs and constant PDE activity in the cytosol, the solution of the stationary reaction-diffusion equation (**Methods S1** for delineation of formulas) indicates that increases of cAMP concentrations in direct vicinity of receptors should dissipate away from the receptors according to a simple 1/r dependency until they reach the cAMP levels of the bulk cytosol.

Based on the data in **Figures 3B, E**, we calculated the increases in cAMP concentrations at the GLP-1R, at 30 and 60 nm distance, and in the bulk cytosol upon stimulation with 1 pM GLP-1 (**Figure 7B**, magenta). Fitting cAMP levels at the receptor and the cytosol (Eq. 1 in **STAR Methods**) strikingly revealed that cAMP concentrations at the 30 nanometer distance (and less so at 60 nanometer distance) from the receptor are much higher than predicted from a 1/r dependency and thereby cannot be explained by simple diffusion and cytosolic bulk PDE concentration alone (**Figure 7B** and **Methods S1**).

At higher agonist concentrations (i.e. 1 nM GLP-1, **Figure 3C,F**), cAMP increases much more at both 30 nm and 60 nm distance and cAMP nanodomains appear to broaden (note that at 1 nM GLP-1 Δ[cAMP] is equal at GLP-1R and at 30 nm distance, **Figure 7B,** blue). Given the much higher receptor occupancy at this agonist concentration, and, therefore, a reduced distance between individual active receptors, isolated cAMP concentration profiles can no longer be assumed; instead, the concentration profiles are expected to become more complex in this situation (c.f. **Eq. 2** in **Methods S1**). In any case, also at high GLP-1 concentrations, it is obvious that cAMP-increases at the receptor do not decrease in space obeying a 1/r distance dependency as would be expected for simple diffusion and constant cytosolic PDE activities (**Figure 7B**).

Our experimental data and quantitative considerations based on the physics of diffusion suggest at least two mechanisms that may explain the shape of the RAINs concentration profiles. First, the diffusion coefficient of cAMP within RAINs might be dramatically reduced over a range of a few tens of nanometers from the receptor. A possible – albeit entirely hypothetical – cellular basis conferring extremely slow diffusion would be molecular crowding or formation of biomolecular condensates. Second, the local concentration of cAMP-degrading PDEs is substantially increased within RAINs compared to the bulk cytosol. The second mechanism would be in line with our experimental data in single cells showing that the effect of PDE inhibition within RAINs is highly different dependent on the distance from the receptor, suggesting differentially localized PDE activity.

The model (**Figure 7A**) further suggests that upon stronger stimulation, the concentrations of cAMP generated by the strongly stimulated adenylyl cyclases begin to overcome the local PDE capacity. This would result in increasing concentrations of free cAMP that can then diffuse freely and dissipate the cAMP concentration gradients, resulting in broadening and then fusion of individual RAINs and ultimately global increases in cAMP - as required for the stimulation of cytosolic cAMP targets and also changes in gene transcription.

DISCUSSION:

Measuring cAMP at defined distances around individual GPCRs, using the GLP-1 receptor as a model, we have identified *receptor-associated, independent cAMP nanodomains* (RAINs) in intact cells. Low levels of stimulation triggered by 1 pM GLP-1, produce a localized receptor-associated cAMP pool that extends up to 60 nm from the receptor. This cAMP pool directly translates into localized, receptor-associated PKA activity and, hence, constitutes a self-sufficient and independent signaling unit. The required presence of PKA regulatory subunits inside RAINs suggests the requirement for localized binding and buffering of cAMP, which would keep the cAMP local and, moreover, enables localized PDEs to shape the size of GPCR-associated cAMP nanodomains. Experiments with the β_2-AR showed similar localized cAMP responses to low levels of stimulation and suggest that RAINs may be a general phenomenon of GPCRs.

Our data suggest that cells may use these RAINs to spatially limit distinct cAMP signals stemming from different GPCRs. This is based on three main findings: First, cAMP concentrations inside RAINs do not equilibrate with cytosolic cAMP over minutes. Second, cAMP pools generated by β_2-ARs do not equilibrate with the cAMP pool inside the GLP-1R nanodomains, i.e. RAINs are protected from (low levels of) stimulation of other GPCRs. Third, disruption of PKA tethering inside RAINs abolishes the signaling function of this individual unit. We propose that by organizing extracellular GPCR stimuli into RAINs, cells are able to precisely sense which cAMP pool stems from which GPCR. Cells would thereby be capable of orchestrating distinct cAMP pools simultaneously and, ultimately, of relaying them into receptor-specific cell function with high spatial precision.

These findings have important implications for our understanding of GPCR signaling via cAMP. Traditionally, cAMP has been regarded as a freely diffusible messenger and, thus, would increase (or decrease) uniformly within the entire cell upon stimulation of adenylyl cyclase-linked GPCRs. This would mean that cAMP would allow cells to operate only as a

single switch, being turned on or off via uniform cellular cAMP levels. However, the existence of very small and independent cAMP signaling nanodomains around each individual GPCR indicates a huge number of cellular switches, with essentially each single GPCR representing one such unit – enlarging the complexity of cAMP signaling by orders of magnitude. Using an analogy from electronics, this would suggest that cAMP signaling of a cell does not represent a single transistor-like switch, but rather a chip comprising a large number of independent but interacting switches.

The possible number of such individual cAMP "switches" at the cell surface can be roughly estimated if we consider that the RAIN's radius appears to be on the order of 60 nm, i.e. their diameter about 120 nm. In order to assure a "safe" distance between individual switches, they may be placed at distances of ≈200 nm, i.e. a density of at 25/μm^2. Considering that most cells have a surface of several hundred μm^2, this would allow for several thousand independent cAMP "switches".

The molecular details of how such RAINs are shaped remain to be elucidated. Our experimental data and quantitative considerations based on the physics of diffusion suggest at least two possible mechanisms. First, a marked reduction of the cAMP diffusion coefficient over a range of a few tens of nanometers from the receptor, which might be brought about by mechanisms such as molecular crowding or formation of biomolecular condensates (Bock et al., 2020; Zhang et al., 2020). Second, substantially higher PDE concentrations close to receptors compared to the bulk cytosol, a mechanism that would be in line with our data showing that PDE inhibition is highly dependent on the distance from the receptor, suggesting differentially localized PDE activity (**Figure 4**).

The exact composition of RAINs, i.e. which proteins contribute to them, how they are organized and whether they are stable or dynamic, also remain to be studied. While our data indicate that AKAPs, PKA and PDEs are necessary constituents, other proteins may well contribute to the individual properties of individual RAINs.

Our model (**Figure 7A**) further suggests that upon stronger stimulation, the concentrations of cAMP generated by the strongly stimulated adenylyl cyclases begin to overcome the local PDE capacity. This would cause dissipation and progressive fusion of the individual RAINs, resulting ultimately in generalized increases of cAMP throughout a cell, which allows generalized activation of cAMP targets including changes in gene transcription via cAMP response elements – processes that would appear to be unrelated to complex signaling via individual RAINs.

The level of receptor stimulation required to overcome RAINs should depend on a number of parameters. For example, comparison of cytosolic cAMP signals induced by low levels of endogenous β_2-AR in HEK cells and those seen upon overexpression of β_2-AR illustrates that receptor levels have a strong impact (compare e.g. **Figure 2E** and **Figure 6D**). Likewise, the agonist concentration affects not only the amplitude but also the kinetics of cAMP signals in the different compartments (compare e.g. **Figure 3B** and **C**). Levels of other protein components inside RAINs, such as PDEs and AKAPs, will also very significantly contribute to their size, shape and function.

Limitations of the Study

Our study demonstrates the existence of *receptor-associated, independent cAMP signaling nanodomains*, RAINs, for two GPCRs – the class B GLP-1R and the class A β_2-AR. It will be important to study, whether similar principles apply to other GPCRs, notably not only to G_s-coupled receptors that increase cAMP, but also those triggering other signaling pathways. In addition, the cells investigated are relatively simple cell culture lines, and it will be most interesting to see how cells with a more complex architecture, such as neurons or cardiomyocytes, may organize such signaling nanodomains. For example, it may be expected that individual RAINs will fuse at postsynaptic sites, and that they may be unevenly distributed in cells where receptor distribution is not uniform, such as cardiomyocytes (Bathe-Peters et al.,

2021). It will be important to see how stable RAINs may be, i.e. if they change over time, both short and long term. Receptors and signaling proteins are highly mobile (Moller et al., 2020; Sungkaworn et al., 2017), which may result in RAINs moving with individual receptors, or in dynamic changes of RAINs over time. And finally, as noted above, the protein composition and their spatial arrangement will need to be elucidated in order to understand, how RAINs function in detail and how RAINs of different receptors may have specific properties.

Taken together, our study reveals mechanisms how cells can independently process large numbers of receptor signals by spatially restricting cAMP in nanometer size RAINs. Localized cAMP signaling has been suggested by a number of studies to be important for normal cell homeostasis and function. As a consequence, a disruption of localized cAMP signaling has been proposed to be associated with various diseases (Bers et al., 2019; Gold et al., 2013; Nikolaev et al., 2010; Zaccolo et al., 2021; Zhang et al., 2020). Our data reveal the molecular mechanisms how such localized cAMP signaling by individual GPCRs is brought about. They further suggest that modulation of individual receptor-associated cAMP nanodomain signaling may hold therapeutic potential.

ACKNOWLEDGEMENTS:

We thank all members of the Lohse lab for valuable discussions on the manuscript. This work was supported by the German Research Foundation (SFB688-B08) and Elitenetzwerk Bayern, Receptor Dynamics program (to M.J.L.). S.E.A. and J.M were members of the International Doctoral Program “Receptor Dynamics: Emerging Paradigms for Novel Drugs” funded within the framework of the Elite Network of Bavaria. I.M. is an Anne McLaren Research Fellow. This work was supported by the British Heart Foundation PG/15/5/31110 and RG/17/6/32944 (to M.Z.).

AUTHOR CONTRIBUTIONS:

I.M., M.J.L., and A.B. conceived of the study. S.E.A., I.M., M.J.L., and A.B. designed experiments. S.E.A. and C.K. conducted the majority of experiments. S.E.A., C.K., I.M., and A.B. analyzed data. S.E.A. designed, conducted, and analyzed dSTORM experiments with the help of J.M., and K.N. designed, conducted, and analyzed the functional characterization of biosensors. A.K and M.Z. helped with sensor calibration experiments. P.A. contributed to discussion. M.F. developed the quantitative framework for cAMP nanodomains. S.E.A., C.K., K.N., and A.B. prepared figures. A.B. and M.J.L. wrote the paper with contributions from S.E.A., C.K., I.M., K.N., and M.F. All authors edited the manuscript. M.J.L. initiated the project. A.B. and M.J.L. directed overall research.

DECLARATION OF INTERESTS:

The authors have no conflict of interest to declare.

FIGURES AND LEGENDS

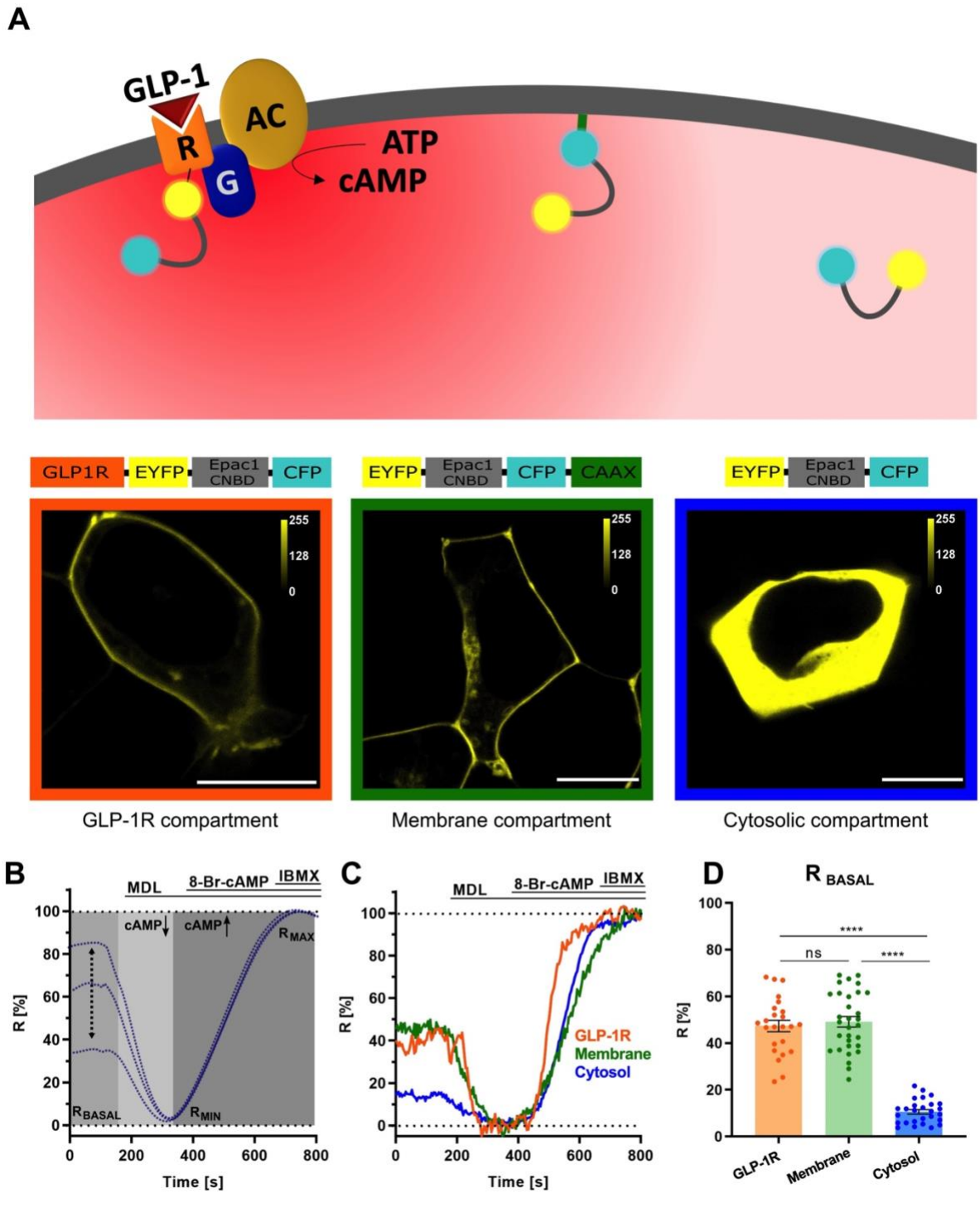

Figure 1. **Targeted cAMP reporters reveal GPCR- and membrane-associated cAMP pools.** (A) Molecular tools to monitor cAMP in different cellular compartments. Upper panel: Targeting of the FRET-based cAMP sensor *Epac1-camps* allows measuring cAMP levels in

the direct vicinity of the GLP-1R, the cell membrane, and bulk cytosol, respectively, in intact cells. R = GLP-1R, G = stimulatory G protein, AC = adenylyl cyclase. Lower panels: Domain structure and cellular localization of *GLP1R-camps* (orange), *Epac1-camps-CAAX* (green), and *Epac1-camps* (blue). CNBD = cyclic nucleotide binding domain. Shown are representative confocal images of HEK cells transiently expressing the indicated constructs. Scale bars = 10 µm. (B) Experimental approach to assess relative cAMP concentrations in different cellular compartments. Shown are simulated traces for 3 different compartments (blue dotted lines). Membrane-bound ACs are inhibited by MDL-12,330A (100 µM) resulting in a decrease of FRET ratio (R_{MIN}). The magnitude of the decrease is dependent on the initial concentration in a cellular compartment (R_{BASAL}, black dotted arrow). Addition of 8-Br-2'-O-Me-cAMP-AM (20 µM) and IBMX (100 µM) saturates *Epac1-camps* (R_{MAX}). FRET traces are normalized to R_{MIN} (set to 0%) and R_{MAX} (set to 100%). The basal cAMP level in a compartment is then directly given by the intersection with the y-axis or calculated by $R_{BASAL}= (R-R_{MIN})/(R_{MAX}-R_{MIN})x100$. (C) Representative time courses of changes in FRET ratio of HEK cells expressing *GLP1R-camps* (orange), *Epac1-camps-CAAX* (green), and *Epac1-camps* (blue) following the protocol described in (B). (D) cAMP levels at GLP-1R are higher than in the bulk cytosol. Quantification of basal cAMP signals from experiments as shown in panel (C). n=24 (*GLP1R-camps*), n=31 (*Epac1-camps-CAAX*), and n=27 (*Epac1-camps*) cells from 8, 8, 10 independent experiments, respectively. The columns represent means, the vertical bars s.e.m. ****$p<0.0001$, according to one-way analysis of variance (ANOVA) with Tukey's post hoc test; ns: not significantly different.

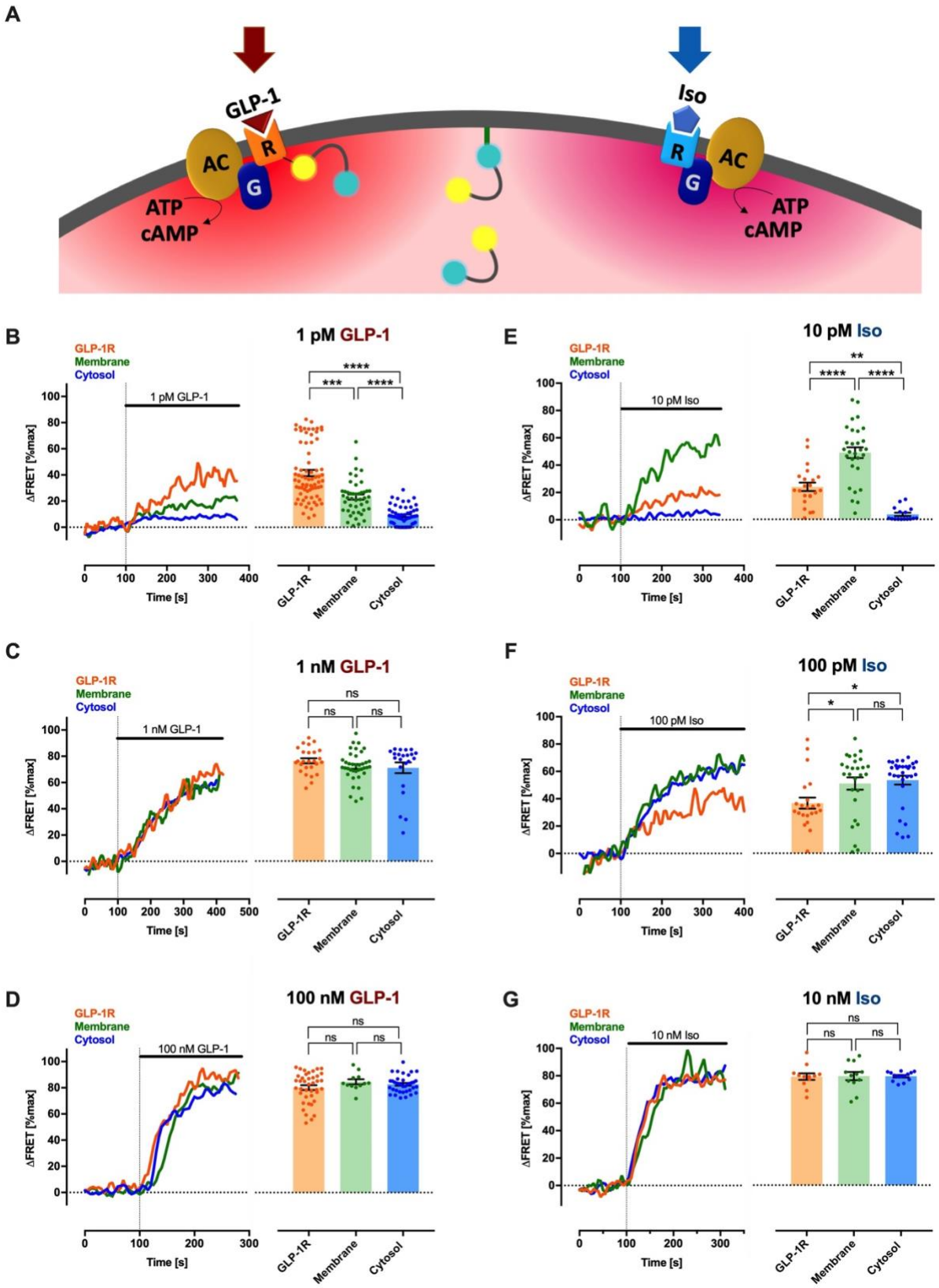

Figure 2. Low-concentrations of GLP-1 exclusively generate a GLP-1R-associated cAMP pool that is protected from a foreign GPCR stimulus (A) Schematic representation of the experimental setup. *Epac1-camps* is targeted to the GLP-1R (orange R symbol), the cell

membrane or the bulk cytosol. Production of cAMP is triggered by either GLP-1 (B-D) or isoproterenol (E-G) upon GLP-1R or endogenous β_2-ARs (blue R symbol) stimulation, respectively. (B-D) Left: Representative traces of corrected and normalized FRET ratios (ΔFRET (%max)) in HEK cells transfected with targeted *Epac1-camps* and treated with 1 pM (B), 1 nM (C), or 100 nM GLP-1 (D). Right: Normalized, GLP-1-induced FRET ratios pooled from all cells measured as in (B-D). The y-axis is the same as shown in the traces on the left and not shown for clarity. FRET traces are normalized to baseline (set to 0%) and maximal stimulation upon FSK (10 μM)/IBMX (100 μM) treatment (set to 100%). (B) n=74 (*GLP1R-camps, orange*), n=45 (GLP-1R + *Epac1-camps-CAAX, green*), n=55 (GLP-1R + *Epac1-camps, blue*) cells from 18, 11, 8 independent experiments, respectively; (C) n=26 (*GLP1R-camps*), n=38 (GLP-1R + *Epac1-camps-CAAX*), n=22 (GLP1-R + *Epac1-camps*) cells from 5, 12, 3 independent experiments, respectively; (D) n=40 (*GLP1R-camps*), n=12 (GLP-1R + *Epac1-camps-CAAX*), n=37 (GLP-1R + *Epac1-camps*) cells from 9, 4, 7 independent experiments, respectively. (E-G) Left: Representative traces of corrected and normalized FRET ratios (ΔFRET (%max)) in HEK cells transfected with the respective targeted *Epac1-camps* sensors and treated with 10 pM (E), 100 pM (F), or 10 nM (G) isoproterenol. Right: Normalized, isoproterenol-induced FRET ratios pooled from all cells measured as in (E-G). The y-axis is the same as shown in the traces on the left and not shown for clarity. FRET traces are normalized to baseline (set to 0%) and maximal stimulation upon FSK (10 μM)/IBMX (100 μM) treatment (set to 100%). (E) n=22 (*GLP1R-camps*), n=29 (GLP-1R + *Epac1-camps-CAAX*), n=16 (GLP-1R + *Epac1-camps*) cells from 6, 7, 3 independent experiments, respectively; (C) n=22 (*GLP1R-camps*), n=27 (GLP-1R + *Epac1-camps-CAAX*), n=31 (GLP-1R + *Epac1-camps*) cells from 4, 7, 6 independent experiments, respectively; (G) n=12 (*GLP1R-camps*), n=12 (GLP-1R+ *Epac1-camps-CAAX*), n=14 (GLP-1R + *Epac1-camps*) cells from 3, 4, 3 independent experiments, respectively. (B-G) The columns represent means, the vertical bars s.e.m. ****$p<0.0001$, ***$p<0.001$, **$p<0.01$ *$p<0.05$ according to one-way

analysis of variance (ANOVA) with Tukey's post hoc test (D,E,G), and according to a Kruskal-Wallis test (B,C,F); ns: not significantly different.

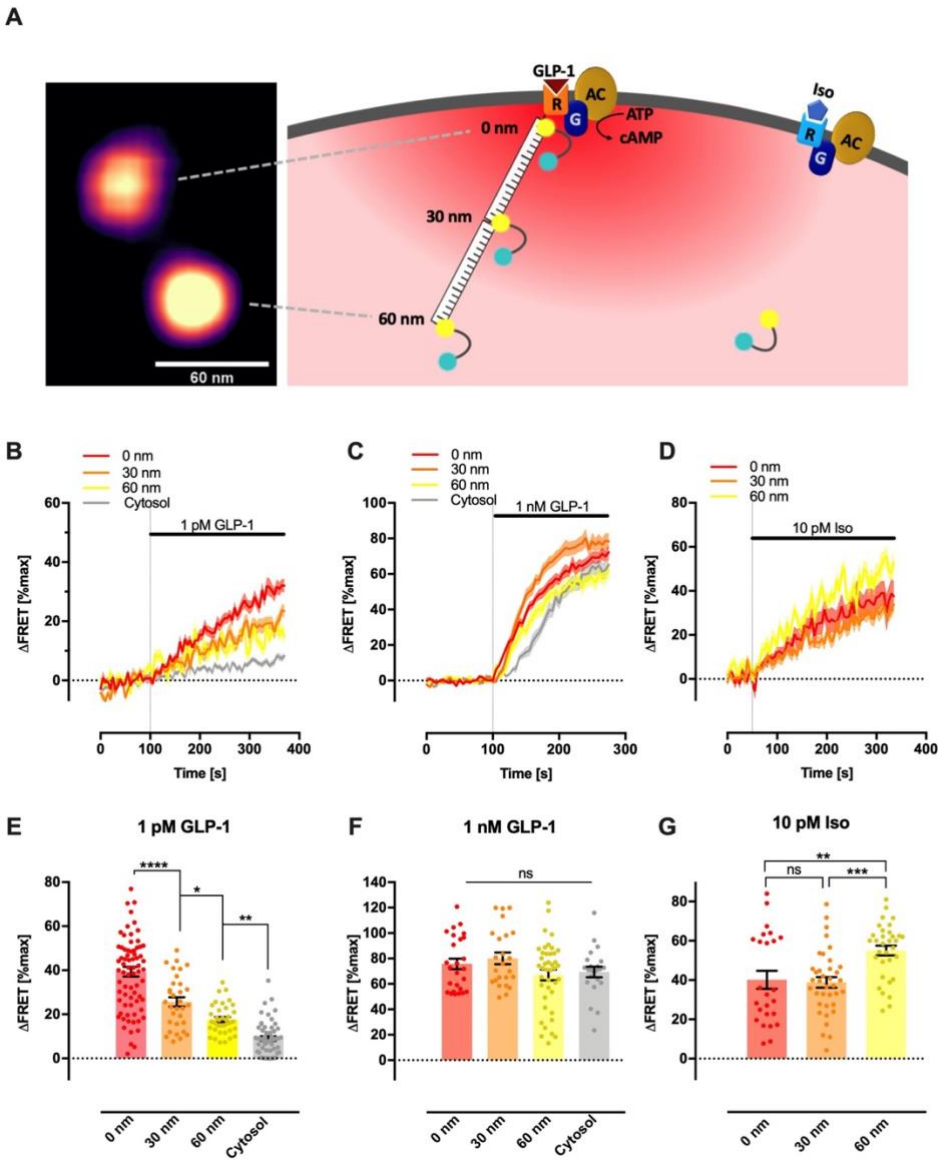

Figure 3. Optical mapping of GLP-1R-associated cAMP pools reveals nanodometer size domains. (A) Genetic incorporation of nanometer size SAH linkers into *GLP1R-camps* allows optical mapping of local cAMP pools in nanometer distances from the receptor. The length of the SAH60 linker was determined by dSTORM (Figure S4). The dSTORM image on the left shows a membrane-bound, representative SAH60 linker molecule flanked by two labeled Halo tags. (B,C,E,F) Mapping of the GLP-1R-associated cAMP pool. (B, C) Averaged traces of corrected and normalized FRET ratios (ΔFRET (%max)) of HEK cells transfected with *GLP1R-camps* (0 nm linker, red), *GLP1R-SAH30-camps* (30 nm linker, orange), *GLP1R-SAH60-camps* (60 nm linker, yellow), or GLP-1R + *Epac1-camps* (cytosol, gray) treated with 1 pM

(B) or 1 nM (C) GLP-1 under basal (i.e. PDEs intact) conditions. FRET traces from each individual cell were normalized to baseline (set to 0%) and the averaged maximal stimulation upon FSK (10 μM)/IBMX (100 μM) treatment (average set to 100%). Solid lines indicate the mean, shaded areas s.e.m. (E,F): Normalized, GLP-1-induced FRET ratios from all cells measured: (B) 1 pM GLP-1: n=74 (0 linker), n=32 (30 nm linker), n=37 (60 nm linker), n=55 (cytosol) cells from 18, 8, 12, and 8 independent experiments, respectively, (C) 1 nM GLP-1: n=26 (0 nm linker), n=24 (30 nm linker), n=41 (60 nm linker), n=22 (cytosol) cells from 5, 5, 9, 3 independent experiments, respectively. (D,G) Mapping of spatial protection of the GLP-1R-associated cAMP pool from a foreign GPCR stimulus. (D) Averaged traces of corrected and normalized FRET ratios (ΔFRET (%max)) in HEK cells transfected with *GLP1R-camps* (0 nm linker, red), *GLP1R-SAH30-camps* (30 nm linker, orange), or *GLP1R-SAH60-camps* (60 nm linker) stimulated with 10 pM isoproterenol. FRET traces from each individual cell were normalized to baseline (0%) and maximal stimulation upon FSK (10 μM)/IBMX (100 μM) treatment (set to 100%). Solid lines indicate the mean, shaded areas s.e.m. (G) Normalized, isoproterenol-induces FRET ratios from n=25 (0 nm linker), n=37 (30 nm linker), n=33 (60 nm linker) cells from 5, 8, 7 independent experiments, respectively. (E-G) The columns represent means, the vertical bars s.e.m. ****$p<0.0001$,***$p<0.001$, **$p<0.01$,*$p<0.05$ according to one-way analysis of variance (ANOVA) with Tukey's post hoc test; ns: not significantly different.

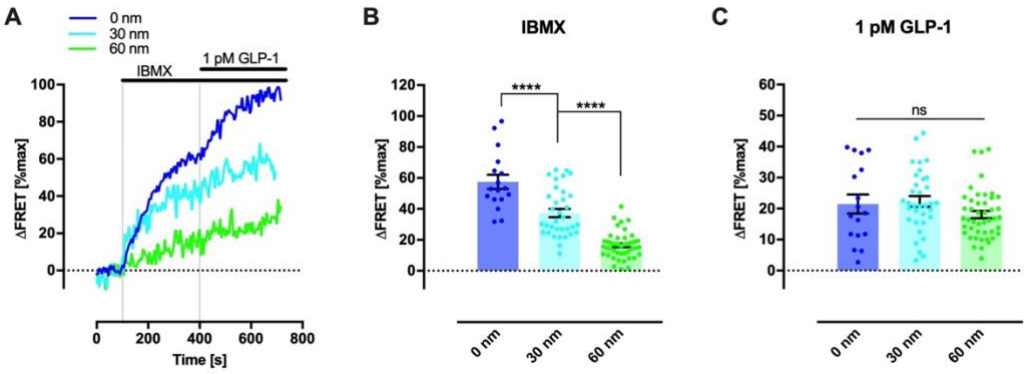

Figure 4. **Localized PDE activity shapes the size of GLP-1R-associated cAMP nanodomains. (**A**)** Inhibition of PDE activity differentially increases cAMP levels in the vicinity of GLP-1R and at 30 and 60 nm distance. Shown are representative traces of corrected and normalized FRET ratios (ΔFRET (%max)) in HEK cells transfected with *GLP1R-camps* (0 nm linker, blue), *GLP1R-SAH30-camps* (30 nm linker, turquoise), or *GLP1R-SAH60-camps* (60 nm linker, green) treated sequentially with 100 µM IBMX and 1 pM GLP-1. FRET traces are normalized to baseline (set to 0%) and the average maximal stimulation upon FSK (10 µM)/IBMX (100 µM) treatment (set to 100%). (B,C) Normalized, IBMX- (B) and GLP-1-induced (C) FRET ratios pooled from all cells measured: n=17 (0 linker), n=34 (30 nm linker), n=45 (60 nm linker) cells from 5, 9, and 12 independent experiments, respectively. The columns represent means, the vertical bars s.e.m. ****$p<0.0001$, according to one-way analysis of variance (ANOVA) with Tukey's post hoc test (B), and a Kruskal-Wallis test (C); ns: not significantly different.

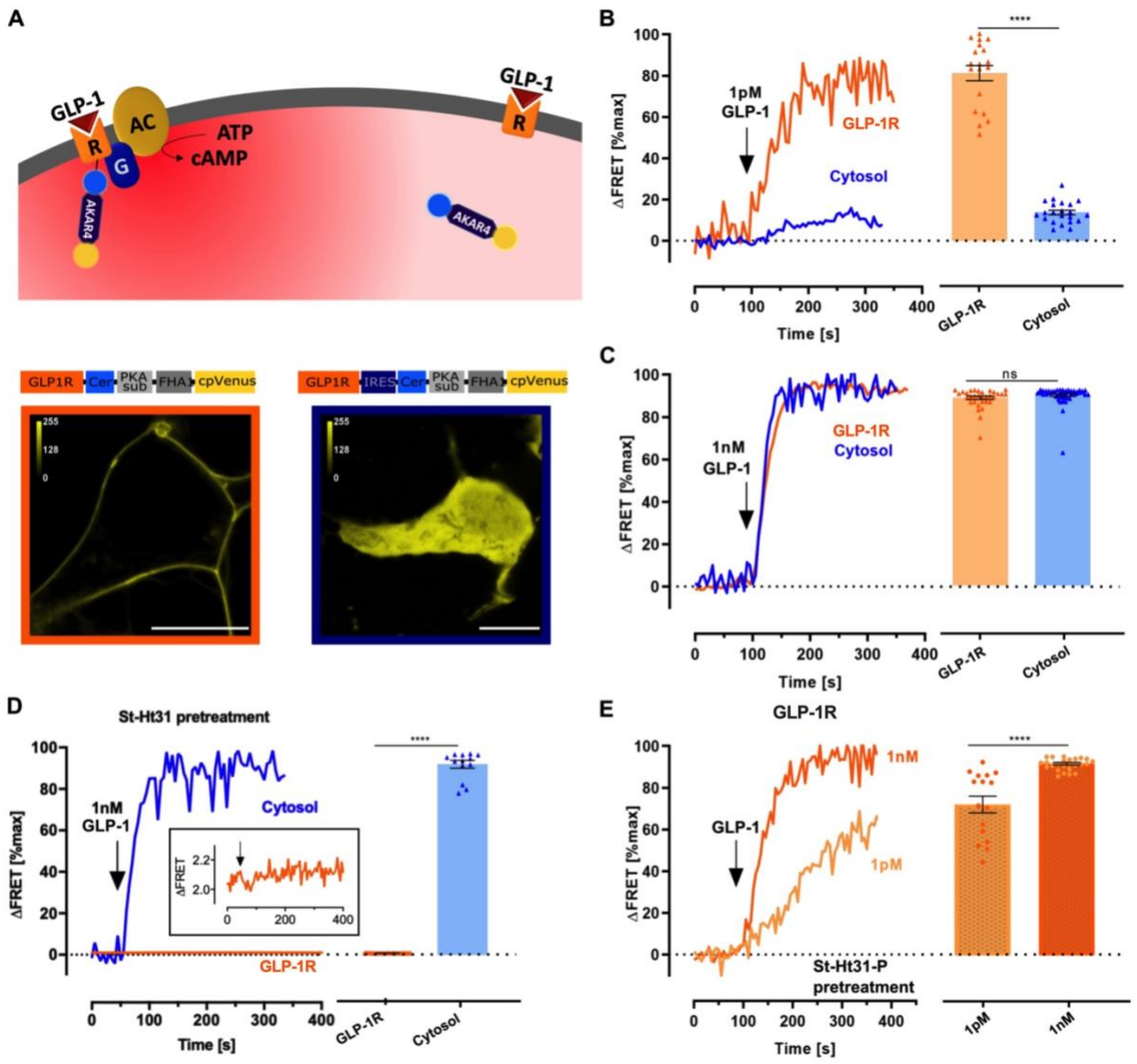

Figure 5. **GLP-1R-associated cAMP nanodomain signaling requires tethered PKA.** **(**A**)** Experimental approach to monitor cAMP nanodomain-driven PKA phosphorylation. Targeting of A-kinase activity reporter 4 (*AKAR4*) to the GLP-1R or separate stoichiometric expression of cytosolic *AKAR4* and GLP-1R allows measuring local and global cytosolic PKA phosphorylation upon GLP-1R activation, respectively. Domain structures and cellular localization of *GLP1R-AKAR4* (lower left panel) and GLP-1R + *AKAR4* (via transfection of GLP1R-IRES-AKAR4, i.e. separate but stoichiometric expression; lower right panel). Shown are representative confocal images of HEK cells transiently expressing the indicated constructs. Scale bars = 10 µm. **(**B,C) Representative traces of corrected and normalized FRET ratios

(ΔFRET (%max)) in HEK cells transfected with *GLP1R-AKAR4* (orange) and *GLP1R-IRES-AKAR4* (blue) and treated with 1 pM (B) or 1 nM GLP-1 (C). FRET traces are normalized to baseline (set to 0%) and maximal stimulation upon FSK (10 µM)/IBMX (100 µM) treatment (set to 100%). Right: Normalized GLP-1-induced FRET ratios indicating GLP-1R nanodomain (orange) or global cytosolic (blue) PKA phosphorylation from all cells; (B) n=19 (*GLP1R-AKAR4*), n=22 (GLP-1R + *AKAR4*) cells from 9 and 4 independent experiments, respectively; (**C**) n=25 (*GLP1R-AKAR4*), n=29 (GLP-1R + *AKAR4*) cells from 8 and 4 independent experiments, respectively. **(**D,E**)** Disruption of PKA anchoring completely abolishes GLP-1R-associated cAMP nanodomain signaling. Experiments were done exactly as in (B,C) with pretreatment (30 min) with St-Ht31 (100 µM) (D) or control peptide St-Ht31-P (100 µM) (E). (D) St-Ht31 pretreatment disrupts PKA anchoring and abolishes GLP-1 receptor nanodomain signaling (orange) while global cytosolic PKA phosphorylation (blue) remains unaffected. n=30 (*GLP1R-AKAR4*), n=14 (GLP-1R + *AKAR4*) cells from 9 and 6 independent experiments, respectively. The inset shows original, non-normalized ΔFRET values and further illustrates the lack of response at *GLP1R-camps* displaying (E**)** St-Ht31-P pretreatment does not affect concentration-dependent, GLP-1-stimulated nanodomain PKA phosphorylation. n=16 (1 pM), n=27 (1 nM) cells from 9 and 6 independent experiments, respectively. The columns represent means, the vertical bars s.e.m. ****$p<0.0001$, according to an unpaired t-test; ns: not significantly different.

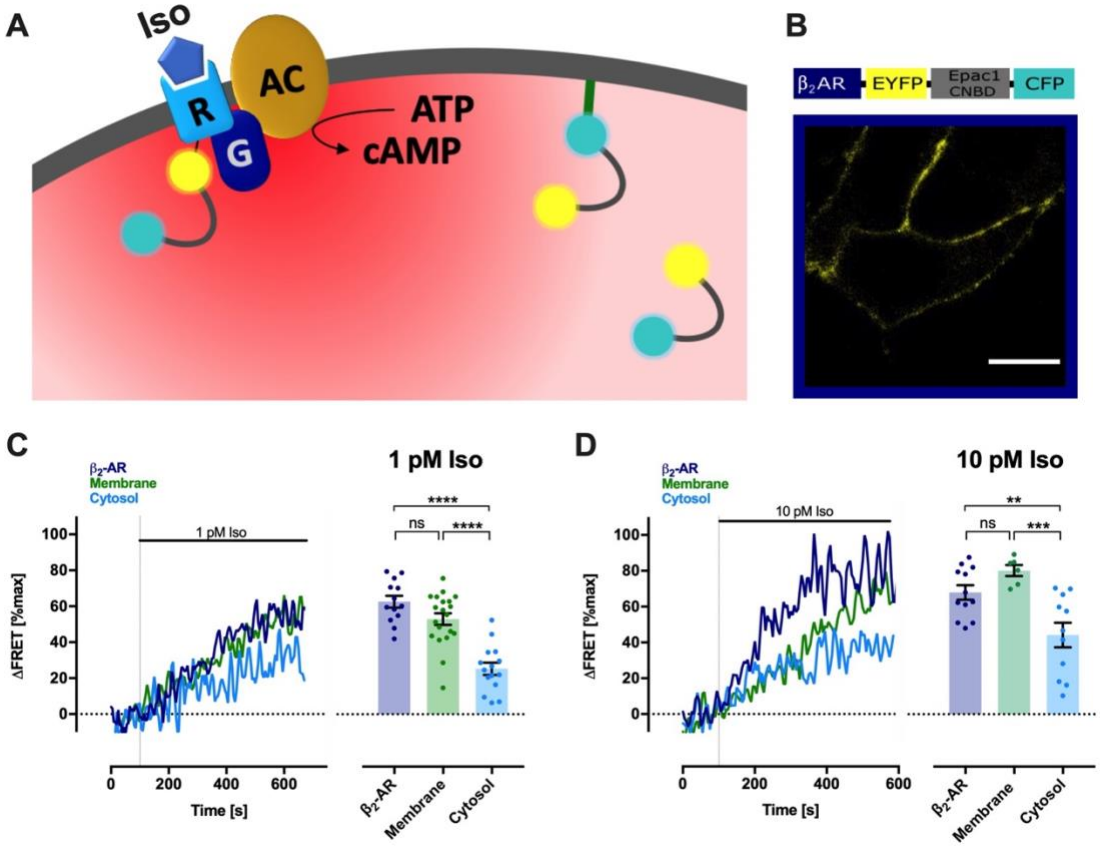

Figure 6: Low-concentration of isoproterenol generates a β2-AR-associated cAMP pool.

(A) Schematic representation of the experimental setup. *Epac1-camps* is targeted to the β2-AR, the cell membrane or the bulk cytosol. Production of cAMP is triggered by isoproterenol. (B) Domain structure and cellular localization of *β2AR-camps*. Shown is a representative confocal image of HEK cells transiently expressing *β2AR-camps*. Scale bar is 10 µm. (C-D) Left: Representative traces of corrected and normalized FRET ratios (ΔFRET (%max)) in HEK cells transfected with targeted *Epac1-camps* and treated with 1 pM (C) or 10 pM (D) isoproterenol. FRET traces are normalized to baseline (set to 0%) and maximal stimulation upon FSK (10 µM)/IBMX (100 µM) treatment (set to 100%). Right (same y-axis as for FRET traces on the left): Normalized, isoproterenol-induced FRET ratios from cells measured as in (C-D). (C) n=13 (*β2AR-camps*), n=20 (β2-AR + *Epac1-camps-CAAX*), n=15 (β2-AR + *Epac1-camps*) cells from 5, 6, 5 independent experiments, respectively; (D) n=12 (*β2AR-camps*), n=6 (β2-AR + *Epac1-camps-CAAX*), n=11 (β2-AR + *Epac1-camps*) cells from 5, 3, 4 independent

experiments, respectively; (C-D) The columns represent means, the vertical bars s.e.m. ****$p<0.0001$ according to one-way analysis of variance (ANOVA) with Tukey's post hoc test; ns: not significantly different.

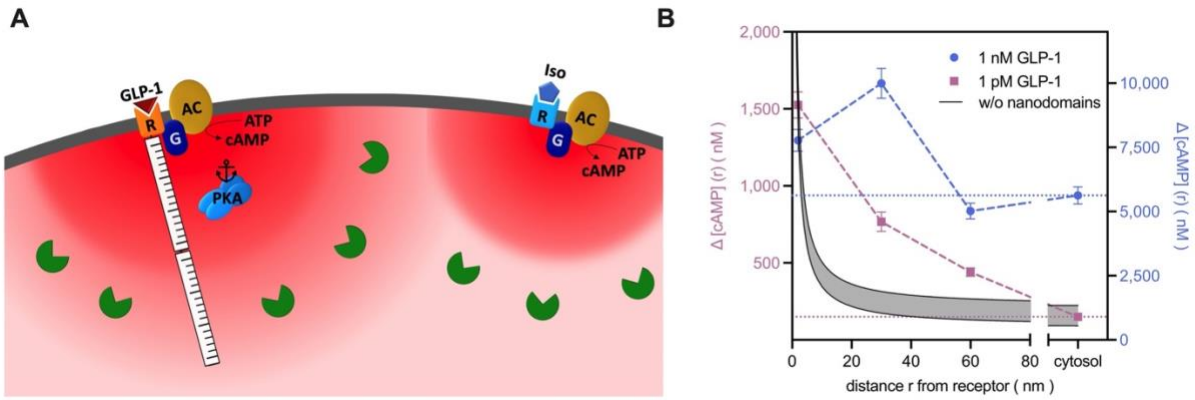

Figure 7: **Model and quantitative considerations of receptor-associated independent cAMP nanodomains (RAINs). (**A**)** Schematic illustration of RAINs: At low agonist concentrations (i.e. low receptor occupancy), GPCRs (e.g. the GLP-1R, left) produce only local cAMP pools (red gradient) in their immediate vicinity that decrease at nanometer distances away from the GPCRs. Importantly, these local cAMP pools have a radius of several tens of nanometers, appear not to overlap with RAINs of other receptors (e.g. β_2-ARs, right), and are shaped by localized PDE activity (green symbols). Within such RAINs, high local concentrations of cAMP cause strong activation of tethered downstream effectors such as PKA (anchor symbol to illustrate the presence of AKAP proteins). At high agonist concentrations (i.e. higher receptor occupancy), RAINs increase in size and begin to merge, resulting in dissipation of cAMP gradients and, ultimately, in a generalized cellular cAMP response. (B) Quantitative considerations of RAINs: cAMP concentration gradients do not obey the laws of simple diffusion. GLP-1-induced FRET changes of the four biosensors (c.f. **Figure 3**) were converted into nanomolar cAMP increases ([ΔcAMP]) and plotted for 1 pM (magenta squares, left y-axis) and 1 nM GLP-1 (blue circles, right y-axis). Dashed lines connecting the data points are meant as a guide to show the geometry of RAINs at both GLP-1 concentrations. Horizontal dotted lines represent cytosolic cAMP after stimulation with 1 pM (magenta) and 1 nM GLP-1 (blue). The gray area displays the mean +/- 95% CI of a fit (A(nM*nm) = 1376 [1306;1446]) assuming a 1/r dependency of the cAMP concentration (see main text, **STAR Methods**, and **Methods S1**).

STAR METHODS

RESOURCE AVAILABILITY

Lead contact

Further information and request for resources and reagents should be directed to and will be fulfilled by the Lead contact Martin J. Lohse (m.lohse@mdc-berlin.de).

Materials availability

Plasmids generated in this study are available from the authors upon request.

Data and code availability

The published article includes all datasets generated or analyzed during this study.

EXPERIMENTAL MODEL AND SUBJECT DETAILS

HEK-tsA201 (ECACC 96121229, Sigma-Aldrich Chemie GmbH, referred to as HEK cells throughout the manuscript), HEK-293AD (AD-100-GVO-CB, BioCat GmbH, Heidelberg, Germany, referred as HEK-AD cells throughout the manuscript) and CHO-K1 cells (CCL-61™, ATCC, Teddington, UK, referred to as CHO cells throughout the manuscript) were cultured in complete DMEM (PAN Biotech, Aidenbach, Germany), or DMEM/Ham's F12 (Life Technologies GmbH, Darmstadt, Germany) respectively, both supplemented with 10 %(v/v) fetal bovine serum, 100 U/ml Penicillin, 100 µg/ml Streptomycin (Pen/Strep, GIBCO Life technologies, Carlsbad, CA, USA) and 2 mM L-glutamine (PAN Biotech, Aidenbach, Germany) at 37 °C and 5% CO_2. Cells were passaged in T75 flasks every 2-4 days when reaching a confluency of 80-90%. Cells were routinely tested for mycoplasma contamination using MycoAlert™ Mycoplasma Detection Kit from Lonza (Basel, Switzerland). Cell lines were not contaminated with mycoplasma.

For fluorescence microscopy experiments, HEK cells and HEK-AD cells (used for β_2-AR biosensors) were seeded on Poly-D-Lysine-coated 24 mm glass cover slips in 6-well plates and transfected with 300-400 ng DNA per cover slip using Effectene transfection reagent (Qiagen, Hilden, Germany) according to the manufacturer's instructions. Culture medium was renewed 24 hours after transfection. Fluorescence microscopy experiments were performed 24-48 hours (*β_2AR-camps, β_2AR-IRES2-Epac1-camps, β_2AR-IRES2-Epac1-camps-CAAX, GLP1R-camps*, *GLP1R-AKAR4*, *GLP1R-IRES2-AKAR4*, *Epac1-camps*, and *Epac1-camps-CAAX*) or 64 hours (*GLP1R-SAH30-camps* and *GLP1R-SAH60-camps*) after transfection.

For sensor calibration experiments CHO cells were seeded on uncoated cover slips into 6-well plates and transfected with 2 µg DNA per cover slip using FuGENE transfection reagent (Promega) according to the manufacturer's protocol. 24 hours after transfection culture medium was renewed and fluorescence microscopy experiments were conducted 48 hours post transfection.

For dSTORM imaging, CHO cells were seeded the night before on uncoated cover slips into 6-well plates. 12-14 hours after seeding, cells were transfected with 2 µg DNA per cover slip using Effectene transfection reagent according to the manufacturer's protocol. 4-5 hours after transfection cells were labelled and fixed. dSTORM experiments were conducted on the same day or 24 hours later.

For cAMP determinations by ELISA, HEK cells were seeded at a density of $2.5x10^5$ cells/well into 6 well plates and left to adhere overnight. Cells were transfected with either wild type GLP-1R or *GLP1R-camps* using a calcium phosphate transfection protocol (3 µg cDNA, 3 µg empty pcDNA3, 125 mM $CaCl_2$, 25 mM N,N-bis[2-hydroxyethyl]-2-aminoethanesulfonic acid, 140 mM NaCl, 0.75 mM Na_2HPO_4 x 2 H_2O, pH=6.95 adjusted at 20°C) incubation for 20 minutes, adding to the cells). 24 hours after transfection culture medium was renewed.

For HTRF experiments to determine cAMP accumulation by GLP-1R biosensors, HEK cells were seeded at a density of 1.3 x 10^6 cells into a 6 cm dish and left to adhere overnight. Cells

were transfected after 24 hours with 6 µg of cDNA using Lipofectamine™ 3000 (Invitrogen™), according to the manufacturer's protocol. On the next day medium was renewed.

For HTRF experiments to determine cAMP accumulation by β_2-AR biosensors, CHO cells were seeded at a density of 4 x 10^5 cells/well into a 6-well plate and left to adhere overnight. Cells were transfected after 24 hours with 2 µg of cDNA using Lipofectamine™ 2000 (Invitrogen™), according to the manufacturer's protocol. 6 hours after transfection medium was renewed.

For PKA phosphorylation assays using *AKAR4* biosensors, HEK cells were seeded at a density of 1.3 x 10^6 into a 6 cm dish and left to adhere overnight. Cells were transfected after 24 hours with 1,5 µg cDNA using Effectene transfection reagent according to the manufacturer's protocol. On the next day medium was renewed.

METHOD DETAILS

Biosensor construction

All cAMP sensor constructs were cloned into pcDNA3. The cDNA for the wildtype human GLP-1R (a kind gift from Dr. Christoph Klenk, University of Zürich, Switzerland) was cloned in frame into a vector containing EYFP using HindIII and XbaI to generate GLP-1R-EYFP. To insert restriction sites for BmtI and BspEI between the GLP-1R and EYFP as well as restriction sites for EcoRI and NotI at the C-terminus of EYFP, the following primers were used to amplify EYFP (#1: forward: 5'- AAA TCT AGA *GCT AGC* GGG *TCC GGA* GTG AGC AAG GGC GAG GAG - 3'; #2: reverse 5'- AAA A*GC GGC CGC* AAA *GAA TTC* CTT GTA CAG CTC GTC CAT - 3' priming sequence underlined, restriction sites in italics). In the following step Epac1(E157-E316)-CFP was cloned in frame into GLP-1R-EYFP using EcoRI and NotI thereby creating *GLP1R-Epac1-camps*. *GLP1R-camps-R279E* was generated by replacing Epac1(E157-E316)-CFP in *GLP1R-camps* with (Epac1(E157-E317[R279E])-CFP) using EcoRI and NotI. The 30 nm ER/K linker (a kind gift from Dr. Sivaraj Sivaramakrishnan,

University of Minnesota, Minneapolis, USA) and 60 nm ER/K linker (synthesized by Eurofins genomics, Ebersberg, Germany) were inserted between GLP-1R and *Epac1-camps* using restriction enzymes BmtI and BspEI. *Epac1-camps-CAAX* was generated starting from *Epac2-camps-CAAX*. CFP-CAAX was cut out using XbaI and XhoI and inserted into *Epac1-camps* instead of the original CFP.

AKAR 4 was a kind gift from Dr. Jin Zhang, University of California San Diego, USA. *GLP1R-AKAR4* and *GLP1R-IRES2-AKAR4* were generated by Gibson cloning (Gibson et al., 2009). For *GLP1R-AKAR4* the insert GLP-1R was PCR amplified using a pair of primers (#3: forward: 5'- CCC AAG CTT GCG GCC GCC ACC ATG GCC GGC GCC CCC GGC - 3', #4: reverse: 5' - GCT CAC CAT GGG ATC CTT ATC TCC GGA CCC GCT AGC TCT AGA - 3'), and inserted upstream of *AKAR4* in its vector (#5: forward: 5' - TCT AGA GCT AGC GGG TCC GGA GAT AAG GAT CCC ATG GTG AGC - 3', #6: reverse: 5' - CGG GCC GGG GGC GCC GGC CAT GGT GGC GGC CGC AAG CTT - 3'). For *GLP1R-IRES2-AKAR4* an IRES2 sequence was PCR amplified as an insert using indicated primers (#7: forward: 5' - AGA GCT AGC GGG TCC GGA TAA GCC CCT CTC CCT CCC - 3', #8: reverse: 5' - CTC GCC CTT GCT CAC CAT TGT GGC CAT ATT ATC ATC - 3'). IRES2 was then inserted between GLP-1R and *AKAR4* in the construct *GLP1R-AKAR4* (#9: forward: 5' - GAT GAT AAT ATG GCC ACA ATG GTG AGC AAG GGC GAG - 3', #10: reverse: 5' - GGG AGG GAG AGG GGC TTA TCC GGA CCC GCT AGC TCT - 3').

For *GLP1R-IRES2-Epac1-camps* and *GLP1R-IRES2-Epac1-camps-CAAX*, the sequence encoding GLP1R-IRES2 from the template *GLP1R-IRES2-AKAR4* was PCR amplified using indicated primers (#11: forward: 5' – CTC ACT ATA GGG AGA CCC AAG CTT ATG GCC GGC GCC CCC GGC CCG CTG – 3', #12: reverse: 5' – CAG CTC CTC GCC CTT GCT CAC CAT TGT GGC CAT ATT ATC ATC GTG TTT – 3'*).* GLP1R-IRES2 was then inserted upstream of *Epac1-camps* or *Epac1-camps-CAAX* in its respective vector (#13: forward: 5' - AAA CAC GAT GAT AAT ATG GCC ACA ATG GTG AGC AAG GGC GAG GAG CTG –

3', #14: reverse: 5' – CAG CGG GCC GGG GGC GCC GGC CAT AAG CTT GGG TCT CCC TAT AGT GAG – 3'). To generate *β2AR-Epac1-camps*, in a first step, the upstream haemagglutinin signal peptide and downstream BmtI and BspEI restriction sites were inserted into a human β_2-AR wild-type sequence by PCR amplification and Gibson cloning using indicated primers (#15: forward: 5' - ATA GGG AGA CCC AAG CTT ATG AAG ACC ATC ATC GCC CTG AGC TAC ATC TTC TGC CTG GTG TTC GCC ATG GGG CAA CCC GGG AAC – 3', #16: reverse: 5' – AAA TCC GGA CCC GCT AGC CAG CAG TGA GTC ATT TGT -3'). In a second step, this β_2-AR sequence was inserted into the *GLP1R-camps* template – where it replaced the GLP-1R wild-type sequence – using restriction enzyme cloning.

To clone *β2AR-IRES2-Epac1-camps* and *β2AR-IRES2-Epac1-camps-CAAX*, the β_2-AR sequence was PCR amplified using indicated primers (#17: forward: 5' – CTC ACT ATA GGG AGA CCC AAG CTT ATG AAG ACC ATC ATC GCC CTG AGC – 3', #18: reverse: 5' – TAG GGG GGG GGG AGG GAG AGG GGC TTA TCC GGA CCC GCT AGC CAG CAG TGA – 3'). β_2-AR was then inserted upstream of *IRES2-Epac1-camps* and *IRES2-Epac1-camps-CAAX* in its vectors *GLP1R-IRES2-Epac1-camps and GLP1R-IRES2-Epac1-camps-CAAX,* respectively, using the following pair of primers (#19: forward: 5' – TCA CTG CTG GCT AGC GGG TCC GGA TAA GCC CCT CTC CCT CCC CCC CCC CTA - 3', #20: reverse: 5' – GCT CAG GGC GAT GAT GGT CTT CAT AAG CTT GGG TCT CCC TAT AGT GAG – 3'). Lyn-Halo-SAH60-Halo-CAAX was synthesized by Genescript, Piscataway, USA. All *AKAR4* constructs and Lyn-Halo-SAH60-Halo-CAAX were expressed in pcDNA3.1. Sequences were validated by sequencing of each construct by Eurofins or LGC genomics.

Single-cell Foerster Resonance Energy Transfer (FRET) imaging

For single-cell FRET imaging experiments, transfected cells were washed once and maintained in FRET buffer (10 mM HEPES, 140 mM NaCl, 5.4 mM KCl, 1 mM $MgCl_2$, 2 mM $CaCl_2$ (pH=7.4)) at room temperature throughout the experiment. Experiments were conducted on an

Axiovert 200 inverted microscope (Zeiss, Jena, Germany) equipped with an oil immersion objective (plan-NEOFLUAR 63x/1.25), a 505 dcxr beam splitter (Visitron Systems, Puchheim, Germany), a xenon lamp coupled to a high speed polychromator system (Visitron Systems), an iXon Ultra EMCCD camera (Andor, Belfast, UK), and Metafluor 7 software (Molecular Devices, Sunnyvale, CA, USA); or on a Leica DMi8 inverted microscope (Leica Microsystems, Wetzlar, Germany) with an oil immersion objective (HC PL APO 63x/1,40-0,60 oil), a dichroic beamsplitter T505lpxr (Visitron Systems), a xenon lamp coupled to Visichrome high speed polychromator (Visitron Systems), a Photometrics Prime 95B sCMOS camera (Visitron systems) with Optosplit II dual emission image splitter (Cairn research, Faversham, UK), and Visiview 4.0 imaging software (Visitron Systems). Donor excitation occurred at 436 nm for 100 ms every 5 seconds and fluorescent images in the donor and acceptor emission channels (480 nm and 535 nm, respectively) were recorded every 5 seconds. Raw emission intensities were background-corrected by subtracting the fluorescence intensity of a cell-free region. Further, bleed-through of donor emission into the acceptor channel was subtracted as described previously (Borner et al., 2011): For all *Epac1-camps*-based sensors, corrected FRET ratios were calculated as the ratio between background-corrected donor emission (I_{donor}) at 480 nm and background and bleed-through-corrected acceptor emission ($I_{acceptor, corr}$) at 535 nm (I_{donor} /$I_{acceptor, corr}$). For *AKAR4*-based sensors the FRET ratio was calculated as the background and bleed-through-corrected acceptor emission over background corrected donor emission ($I_{acceptor, corr}$ /I_{donor}). Drift corrected FRET traces were normalized (ΔFRET (% max)) to the basal ratio before compound addition (set to 0%) and maximum stimulus elicited by 10 µM forskolin and 100 µM IBMX at the end of each experiment (set to 100 %). Representative FRET traces in **Figures 2, 5 and 6** were smoothed using adjacent average with 2nd order polynomial smoothing function.

Confocal microscopy

Cells were washed once and maintained in FRET buffer. Confocal images were obtained on a Leica TCS SP8 laser scanning microscope with an oil immersion objective (HC PL APO 63x/1,40 oil). A 514 nm laser was used at 5 % power to excite acceptor fluorophores and the respective emission was measured within 520-600 nm. Images were acquired with a hybrid detector in photon counting mode (1024 x 1024 pixel, line average 4, 400 Hz). Confocal images were analyzed using ImageJ. Each image was corrected by subtracting the average background fluorescence. Contrast was enhanced while keeping the saturated pixels at 0.1%.

Direct Stochastic optical reconstruction microscopy (dSTORM)

After labeling cells transiently expressing the SAH60 construct with 1 µM of the HaloTag® ligand JF-646 for 20 minutes at 37°C, they were fixed for 30 minutes with ice-cold methanol at -20°C. During imaging, cells were kept in Glox buffer (0.56 mg/ml glucose oxidase, 34 µg/ml catalase, 10 % glucose, 0.1 M mercaptoethylamine, 50 mM Tris, 10 mM NaCl (pH=8.0)), at room temperature. dSTORM images were acquired on a TIRF illuminated Nikon Eclipse Ti2 microscope (Nikon, Tokyo, Japan) equipped with a 100x objective with a 1.49 NA automated correction collar; 405, 488, 561, 647 nm laser diodes coupled through an automated N-storm module, and four iXON Ultra897 EMCCD Cameras (Andor). For dSTORM imaging, the automated objective collar and the hardware auto-focus were activated. The 647 nm laser was set to a power of 100 % and images were acquired at 80 ms integration time for at least 15000 frames or until blinking events were negligible. dSTORM movies were processed and analyzed in ImageJ using the Thunderstorm plugin (Ovesny et al., 2014).

Sensor calibration

Epac1-camps-based cAMP FRET sensors were calibrated using a saponin permeabilization approach. First, the intracellular pH of HEK cells was assessed as described before (Koschinski and Zaccolo, 2015). Resulting pH value of 7.5 was used in all subsequent steps for intracellular

buffers. Subsequently, the right combination of a KCl- and K-glutamate-based intracellular buffer was assessed in CHO cells resulting in a combination of 45% KCl- + 55% K-glutamate-based buffer, used during all calibration experiments. KCL- and K-glutamate based buffers contained 135 mM KCl/135 mM K-glutamate x H_2O, 10 mM NaCl, 6.49 mM $MgCl_2$ x $6H_2O$, 0.00073 mM $CaCl_2$ x $2H_2O$, 0.5 mM EGTA, 10 mM HEPES (pH=7.5). For calibration, HEK cells were maintained in intracellular buffer at room temperature, 10-12 µg/ml saponin was added to permeabilize the cells, together with a defined concentration of cAMP (range 0-1 mM, one concentration per cover slip).

cAMP ELISA

48 hours after transfection, HEK cells were washed once with FRET buffer and incubated for 25 minutes with GLP-1-(7-36)-NH_2 + 100 µM IBMX (for the concentration response curve), 10 µM Fsk+100 µM IBMX (positive control), 100 µM IBMX (negative control). Cells were lysed before proceeding with the ELISA (cyclic AMP ELISA Kit, Cayman chemicals, Michigan, USA) conducted according to the manufacturer's protocol.

cAMP accumulation assays by HTRF

HEK cells, transfected with GLP-1R biosensors were washed 48 hours after the transfection, trypsinized, resuspended in 1x stimulation buffer and seeded at a density of 800 cells per well into white 96-well low-volume plates (Cisbio). Cells were incubated for 30 min at 37 °C with a concentration range of GLP-1 diluted in 1x stimulation buffer supplemented with 200 µM IBMX (5x *stimulation buffer 1* from the cAMP Gs dynamic kit HTRF (Cisbio) was diluted to 1x with ddH_20, supplemented with 0.2 % BSA (VWR International GmbH), and sterile filtered (pH=7.4)). cAMP accumulation was measured using the cAMP Gs dynamic kit HTRF (Cisbio) according to the manufacturer's protocol.

CHO cells, transfected with β_2-AR biosensors were washed 24 hours after the transfection, trypsinized, resuspended in 1x stimulation buffer and seeded at a density of 4000 cells per well into white 96-well low-volume plates (Cisbio). Cells were incubated for 30 min at 37 °C with a concentration range of isoprenaline diluted in 1x stimulation buffer supplemented with 200 µM IBMX. cAMP accumulation was measured using the cAMP Gs HiRange kit HTRF (Cisbio) according to the manufacturer's protocol. Plate reader experiments were conducted using a Synergy Neo2 plate reader (BioTek, Vermont, USA), equipped with HTRF filter optics. Concentration−effect curves were fitted by a three-parameter logistic function yielding parameter values for a ligand's potency (pEC_{50}).

Forskolin-induced PKA phosphorylation

HEK cells, expressing AKAR4 biosensors were washed 24 hours after the transfection, trypsinized, resuspended and transferred to Poly-D-Lysine-precoated black-wall, black-bottomed 96-well plates (Brand) at a density of 60,000 cells/well. On the next day, cells were washed and medium was replaced with 90 µL FRET buffer. Basal FRET ratio was read for 5 min and subsequently, 10 µL of 10x forskolin dilutions or FRET buffer (negative control) was applied to each well and the FRET ratio was recorded for 20 min. Plate reader experiments were conducted at 37 °C using a Synergy Neo2 plate reader (BioTek, Vermont, USA), equipped with filter optics (excitation filter 420/50 nm; dual emission filter: 485/20 nm - 540/25 nm). FRET ratios were defined as corrected acceptor emission/donor emission. FRET ratios before ligand/buffer addition were averaged and defined as FRETbasal. To quantify ligand-induced FRET changes, ΔFRET was calculated for each well and time point as percent over basal ([(FRETstim− FRETbasal)/FRETbasal] × 100). Subsequently, the average ΔFRET of buffer-treated control wells was subtracted (Schihada et al., 2021). Concentration−effect curves were fitted by a three-parameter logistic function yielding parameter values for a ligand's potency (pEC_{50}).

Quantitative analysis of cAMP gradients at the nanometer scale

In our quantitative considerations (**Methods S1**) we assume a cytosolic PDE concentration of 3 nM and a cAMP diffusion coefficient of D = 100 $\mu m^2/s$ (Bock et al., 2020). Based on this, a constant that describes the decrease of [ΔcAMP] with increasing distance from the source in stationary profiles by cytosolic PDEs is given by 0.17 μm^{-1} (**Methods S1**). Thus, we can neglect cAMP degradation by cytosolic PDEs on the lengthscale of 60 nm.

To quantify how cAMP concentrations at GPCRs decrease over a nanometer range, the [cAMP] values (**Figure 7B**) at GLP-1R and the cytosol were fit to the corresponding solution of the diffusion equation (**Methods S1**)

$$[cAMP] = 2A/r + B, \qquad \text{(Equation 1)}$$

where r denotes the cAMP distance from the receptor, A denotes the cAMP concentration increase above bulk at 2 nm distance from the receptor, and B signifies the cAMP concentration in the cytosol that was constrained to the cytosolic [cAMP] (150 nM).

Statistical analysis

Statistical analyses and curve fitting were performed with Prism 7.0 (or newer) software (GraphPad Software, San Diego, USA) and OriginPro (OriginLab Corporation, Northampton, USA). Normalized FRET ratios are expressed as the mean ± s.e.m.. In single cell experiments, all cells were analyzed separately and plotted as individual symbols in all bar graphs. We refer to the number of individual cells analyzed as n-number, and this n-number was used for statistical analysis. All data were tested for Gaussian distribution using the D'Agostino-Pearson normality test. Differences between means were assessed by a two-tailed student's t-test (for two groups) or a one-way analysis of variance (ANOVA, for three or more groups)

followed by Tukey's post hoc test for normally distributed data and a Kruskal-Wallis test in the case of non-normally distributed data. Details are indicated in respective Figure legends. Differences were considered significant for values of $p<0.05$. P values >0.05 are indicated in the figures as not significantly different (ns). All experiments and representative data shown were repeated at least three times and performed with independent samples.

SUPPLEMENTAL FIGURE TITLES AND LEGENDS

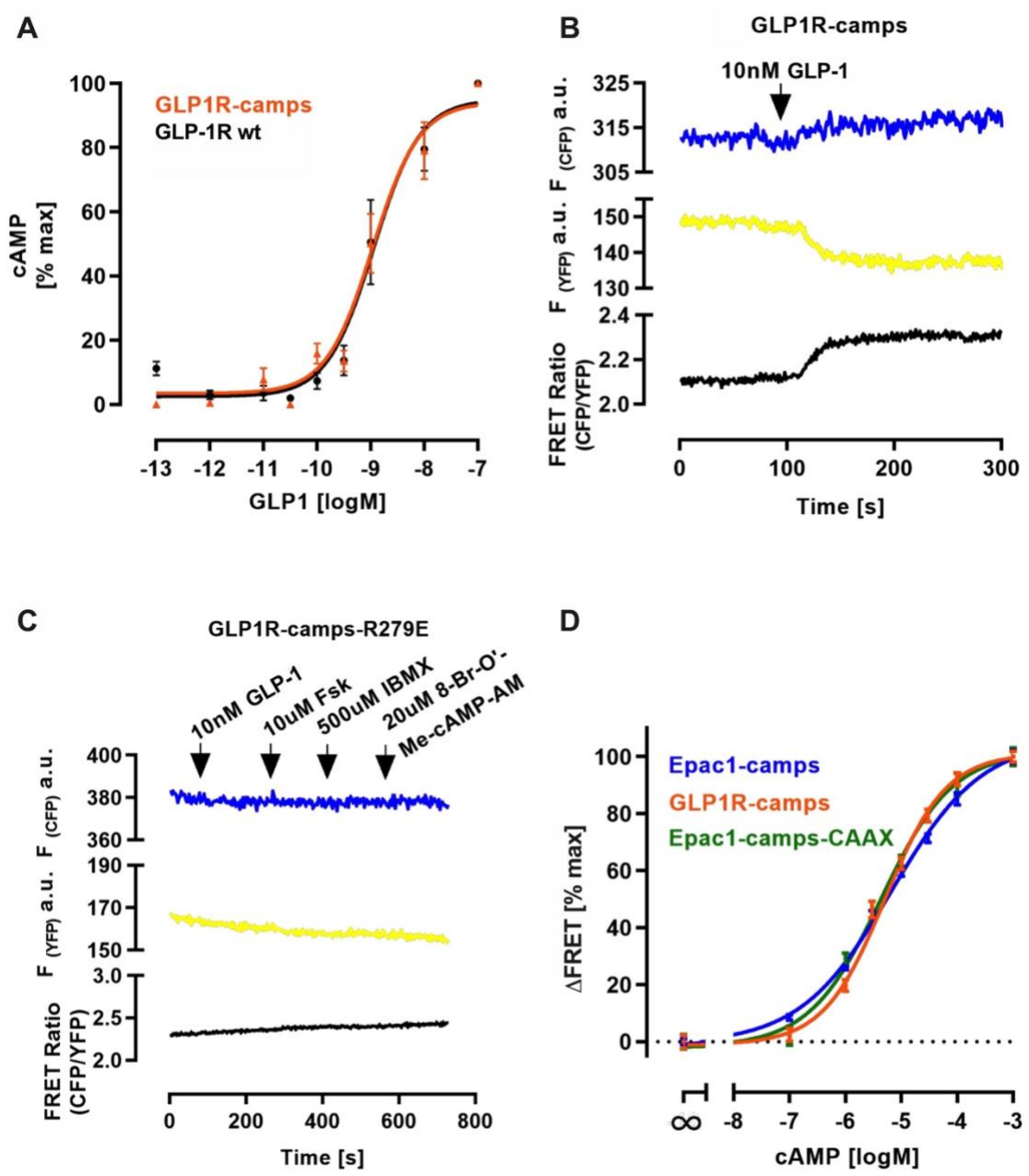

Figure S1. Related to Figure 1. *GLP1R-camps* is a functional GPCR for cAMP sensing. **(**A**),** *GLP1R-camps* is a *bona fide* GPCR that is not compromised with regard to GLP-stimulated whole-cell cAMP production. Shown are concentration-response curves of GLP-1-induced whole-cell cAMP production (measured by ELISA) for *GLP1R-camps* (orange) in comparison to WT-GLP-1R (black). Data were normalized to saturating GLP-1 concentrations and fitted to a three-parameter logistic function yielding similar potencies (pEC_{50}) for GLP-1 at *GLP1R-*

camps (9.02 ± 0.11) and GLP-1R wt (8.99 ± 0.10). Data are means ± s.e.m. from 3 independent experimental days for each construct. **(**B**),** Fluorescence intensity traces of CFP and YFP and resulting FRET ratio (CFP/YFP) recorded in HEK cells transiently expressing *GLP1R-camps*. 10 nM GLP-1 stimulation induces an increase in the CFP and a decrease in the YFP channel, respectively, confirming agonist-induced FRET changes. Traces are representative for 10 cells from 5 independent experiments. (C**),** Fluorescence intensity traces of CFP and YFP and resulting FRET ratio (CFP/YFP) recorded in HEK cells expressing the cAMP binding-deficient *Epac1-camps* mutant R279E fused to the GLP-1R. No changes in fluorescence intensities or FRET ratio are observed upon stimulation with various compounds that lead to cAMP production (indicated in the Figure), or the Epac-specific cAMP analogue 8-Br-O'-Me-cAMP-AM. Traces are representative for 10 cells from 4 independent experiments. (D**)** Attaching *Epac1-camps* to GLP-1 receptors (*GLP1R-camp*s) or targeting it to the membrane (*Epac1-camps-CAAX*) does not impair binding of cAMP. Shown are concentration-response curves generated using HEK cells expressing cytosolic *Epac1-camps* (blue), *GLP1R-camps* (orange) or *Epac1-camps-CAAX* (green) upon upon addition with the indicated cAMP concentrations in the presence of saponin (12 µg/ml). Data are normalized to baseline (no cAMP, set to 0%) and maximal stimulation upon 1mM cAMP infusion (set to 100%). pEC_{50} (mean ± s.e.m.) *Epac1-camps* = 5.2 ± 0.05, *GLP1R-camps* = 5.3 ± 0.05, *Epac1-camps-CAAX*= -5.4 ± 0.09. Data are means ± s.e.m. of 6 independent experimental days for each construct.

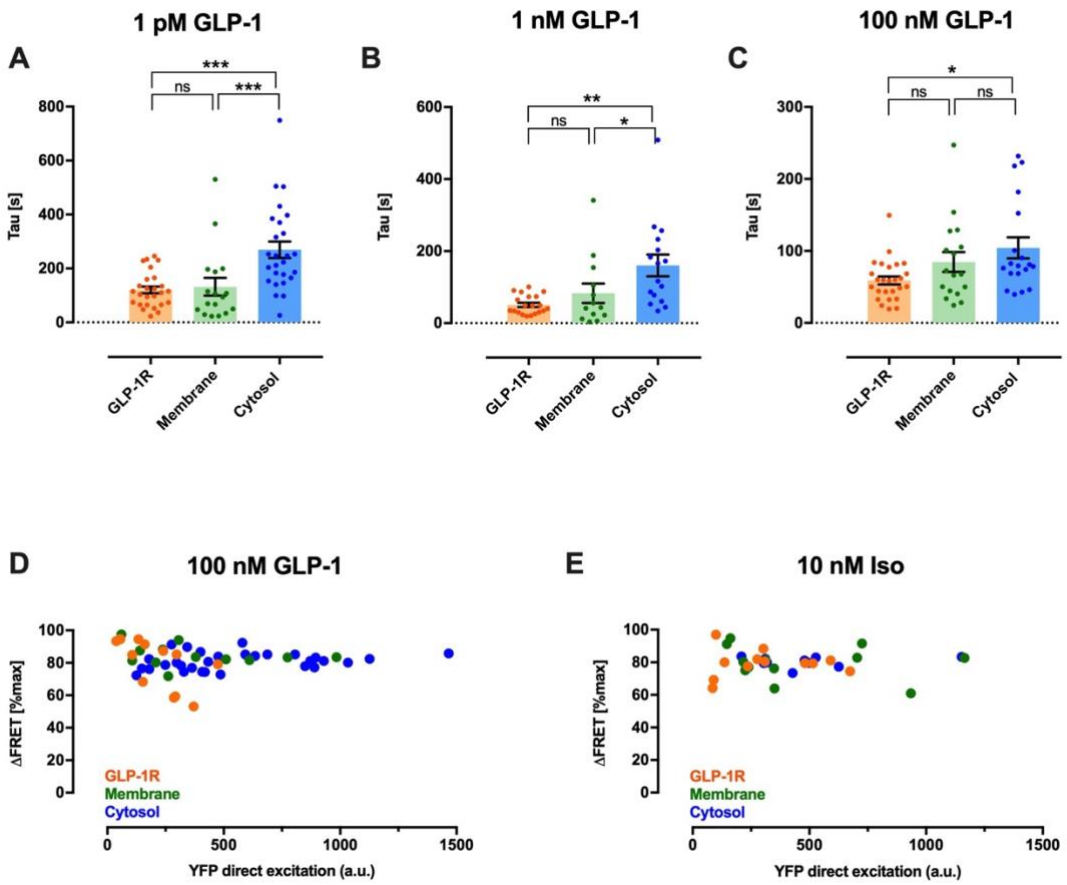

Figure S2. Related to Figure 2. Apparent kinetic constants of GLP-1-induced FRET changes and expression levels of biosensors. (A-C) Apparent kinetic constants (Tau) of FRET changes induced by stimulation with 1 pM (A), 1 nM (B) or 100 nM (C) GLP-1 for the GLP-1R (orange), membrane (green) and cytosolic compartment (blue). GLP-1 was added to the bath and, upon signal onset, FRET traces were fitted to a one-phase exponential association function yielding the indicated kinetic constants. (A) n=26 (*GLP1R-camps*), n=17 (*Epac1-camps-CAAX*), n=26 (*Epac1-camps*) cells from 5, 3, 3 independent experiments, respectively; (B) n=20 (*GLP1R-camps*), n=13 (*Epac1- camps-CAAX*), n=16 (*Epac1-camps*) cells from 4, 7, 5 independent experiments, respectively; (C) n=26 (*GLP1R-camps*), n=17 (*Epac1-camps-CAAX*), n=19 (*Epac1-camps*) cells from 5, 6, 7 independent experiments, respectively. The columns represent means, the vertical bars s.e.m., ***p<0.001, **p<0.01, *p<0.05 according to a Kruskal-Wallis test, ns: not significantly different. (D,E) Ligand-induced FRET responses are independent of expression level of biosensors. Shown are corrected and normalized FRET

ratios induced by the indicated GLP-1 (D) or isoproterenol (E) concentration. HEK cells were transiently transfected with *GLP1R-camps* (GLP-1R, orange), *GLP1R-IRES-Epac1-camps-CAAX* (membrane, green), and *GLP1R-IRES-Epac1-camps* (cytosol, blue). FRET ratios are normalized to baseline (set to 0%) and maximal stimulation upon FSK (10 μM)/IBMX (100 μM) treatment (set to 100%).

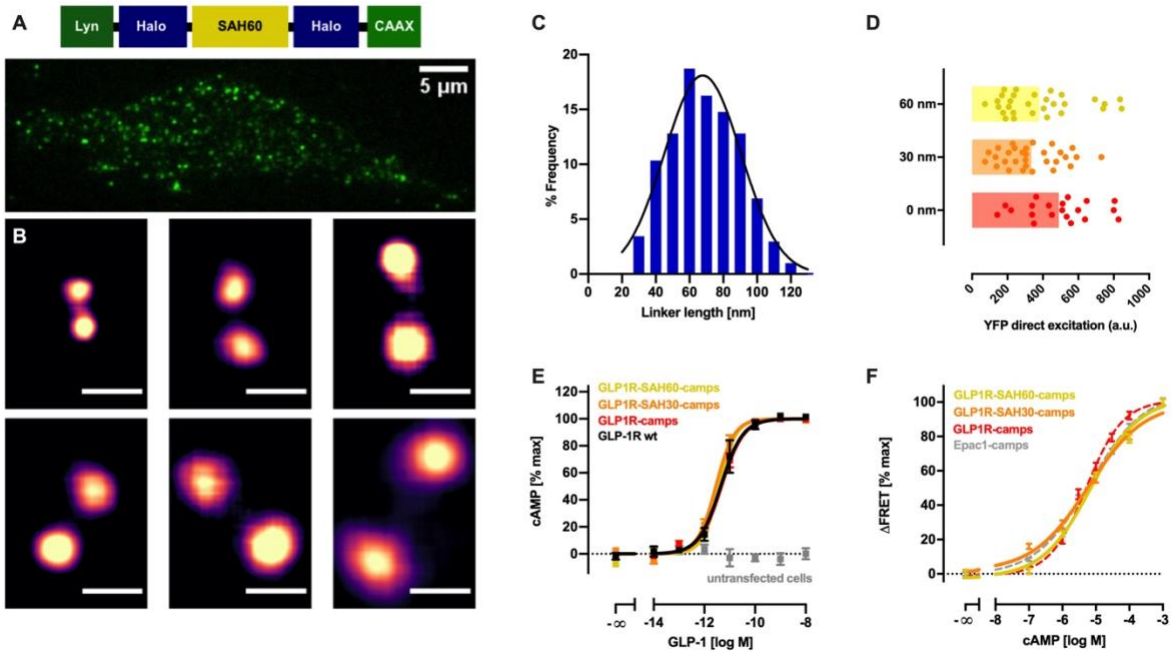

Figure S3. Related to Figure 3. Characterization of GPCR nanorulers. (A) Top: Domain structure of the SAH60 linker construct flanked by two HaloTags, targeted to the cell membrane to perform dSTORM imaging. Bottom: Representative first frame from the localization microscopy stacks of a CHO cell expressing the indicated construct labeled with Halo JF-646, from which the reconstructed super-resolution image was generated. (B) Close-up view of representative linkers containing two Halo JF-646 fluorophores. Scale bar is 60 nm. (C) Histogram depicting the frequency distribution of linker length. Average length is 68.8 ± 1.42 nm. Peak abundance in the histogram is at 60 nm. Data represent mean ± s.e.m. of 203 linkers measured from 10 different cells. (D) Expression levels of all GPCR nanorulers are similar. Shown are EYFP emission values (a.u.) of HEK cells transiently transfected with *GLP1R-camps* (0 nm, red), *GLP1R-SAH30-camps* (30 nm, orange) and *GLP1R-SAH60-camps* (60 nm, yellow). (E) *GLP1R-SAH30-camps and GLP1R-SAH60-camps* are *bona fide* GPCRs that are not compromised with regard to GLP-1-stimulated whole-cell cAMP production. Shown are concentration-response curves of GLP-1-induced whole-cell cAMP production (measured by HTRF, **STAR Methods**) for *GLP1R-SAH60-camps* (yellow), *GLP1R-SAH30-camps* (orange) and *GLP1R-camps* (red) in comparison to GLP-1R wt (black), and

untransfected HEK cells. Data were normalized to saturating GLP-1 concentrations and fitted to a three-parameter logistic function yielding similar potencies (pEC_{50}) for GLP-1 at *GLP1R-SAH60-camp*s (11.4 ± 0.10), *GLP1R-SAH30-camp*s (11.6 ± 0.10), *GLP1R-camps* (11.3 ± 0.10) and GLP-1R wt (11.3 ± 0.20). Data are means ± s.e.m. from 3-4 independent experimental days for each construct. (F) GPCR nanorulers are not impaired in their affinities for cAMP. Shown are concentrations-response curves generated using HEK cells expressing *GLP1R-SAH30-camps* (orange) and *GLP1R-SAH60-camps* (yellow) upon addition of the indicated cAMP concentrations in the presence of saponin (12 μg/ml). Data are normalized to baseline (no cAMP, set to 0%) and maximal stimulation upon 1mM cAMP addition (set to 100%). pEC_{50} (mean ± s.e.m.) *GLP1R-SAH30-camps* = 5.23 ± 0.07, *GLP1R-SAH60-camps* = 5.2 ± 0.07. Data are means ± s.e.m. of 6 and 7 individual experimental days, respectively. *GLP1R-camps* (red) and *Epac1-camps* (gray) are replotted as dashed lines from **Figure S1** for comparison. One-way analysis of variance (ANOVA) with Tukey's post hoc test of all pEC_{50} values (*Epac1-camps, GLP1R-camps, GLP1R-SAH30-camps, and GLP1R-SAH60-camps*) shows no significant difference, $p>0.05$.

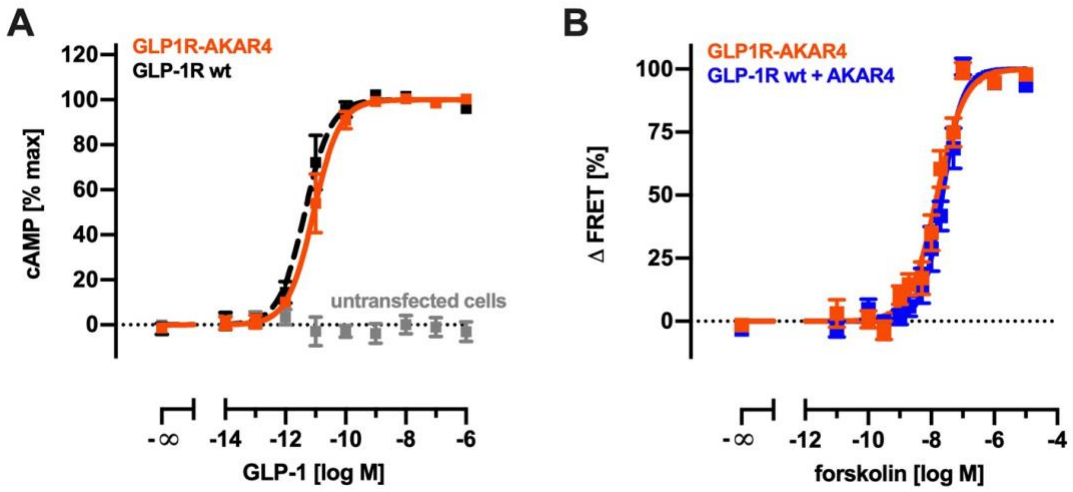

Figure S4. Related to Figure 5. *GLP1R-AKAR4* is functional with regard to cAMP signaling and to PKA phosphorylation sensitivity. (A) *GLP1R-AKAR4* is a *bona fide* GPCR that is not compromised with regard to GLP-1-stimulated whole-cell cAMP production. Shown are concentration-response curves of GLP-1-induced whole-cell cAMP production (measured by HTRF, **STAR Methods**) for *GLP1R-AKAR4* (orange) in comparison to GLP-1R wt (black), and untransfected HEK cells (gray). Data were normalized to saturating GLP-1 concentrations and fitted to a three-parameter logistic function yielding similar potencies (pEC_{50}) for GLP-1 at *GLP1R-AKAR4* (11.0 ± 0.20) and GLP-1R wt (11.3 ± 0.20). Data are means ± s.e.m. from 4 independent experimental days for each construct. Data for GLP-1R wt are re-plotted from **Figure S3**. (B) Tethering *AKAR4* to GLP-1 receptors (*GLP1R-AKAR4*, orange) does not change its phosphorylation sensitivity. Shown are concentration-response curves of forskolin-induced whole-cell PKA activity that is sensed by *AKAR4* (blue) and *GLP1R-AKAR4* (orange), and detected as an increase in FRET (**STAR Methods**). Data were normalized to saturating forskolin concentrations and fitted to a three-parameter logistic function yielding similar potencies (pEC_{50}) for forskolin at *GLP1R-AKAR4* (7.82 ± 0.05) and *AKAR4* (7.65 ± 0.05). Data are means ± s.e.m. from 5 independent experimental days for each construct.

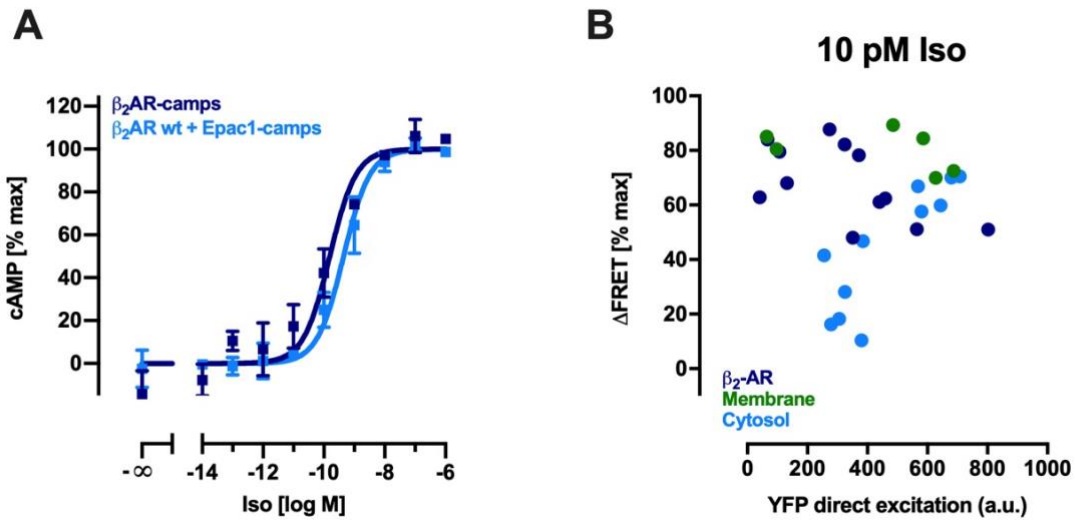

Figure S5. Related to Figure 6. Expression and functional validation of *β2AR-camps*. (A) *β2AR-camps* is a *bona fide* GPCR that is not compromised with regard to isoproterenol(Iso)-stimulated whole-cell cAMP production. Shown are concentration-response curves of Iso-induced whole-cell cAMP production (measured by HTRF, **STAR Methods**) for *β2AR-camps* (dark blue) in comparison to β2-AR wt (light blue). Data were normalized to saturating Iso concentrations and fitted to a three-parameter logistic function yielding similar potencies (pEC_{50}) for Iso at *β2AR-camps* (9.87 ± 0.28) and β2-AR wt (9.37 ± 0.29). Data are means ± s.e.m. from 3 independent experimental days for each construct. (B) Iso-induced FRET responses are independent of expression level of biosensors. Shown are corrected and normalized FRET ratios induced by 10 pM Iso. HEK cells were transiently transfected with *β2AR-camps* (*β2AR*, dark blue), *β2AR-IRES-Epac1-camps-CAAX* (membrane, green), and *β2AR-IRES-Epac1-camps* (cytosol, light blue). FRET ratios are normalized to baseline (set to 0%) and maximal stimulation upon FSK (10 μM)/IBMX (100 μM) treatment (set to 100%).

Protein Name	Helical contour length	Sequence
SAH30	30 nm	GEEEEKKKEEEEKKQKEEQERLAKEEAERKQKEEQERLAKEEAERKQKEEEERKQKEEEERKQKEEEER KLKEEQERKAAEEKKAKEEAERKAKEEQERKAEEERKKKEEEERLERERKEREEQEKKAKEEAERIAKLE AEKKAEEERKAKEEEERKAKEEEERKKKEEQERLAKEKEEAERKAAEEKKAKEEQERKEKEEAERKQRG
SAH60	60 nm	GEEEEKKKEEEEKKQKEEQERLAKEEAERKQKEEQERLAKEEAERKQKEEEERKQKEEEERKQKEEEER KLKEEQERKAAEEKKAKEEAERKAKEEQERKAEEERKKKEEEERLERERKEREEQEKKAKEEAERIAKLE AEKKAEEERKAKEEEERKAKEEEERKKKEEQERLAKEKEEAERKAAEEKKAKEEQERKEKEEAERKQRG GEEEEKKKEEEEKKQKEEQERLAKEEAERKQKEEQERLAKEEAERKQKEEEERKQKEEEERKQKEEEER KLKEEQERKAAEEKKAKEEAERKAKEEQERKAEEERKKKEEEERLERERKEREEQEKKAKEEAERIAKLE AEKKAEEERKAKEEEERKAKEEEERKKKEEQERLAKEKEEAERKAAEEKKAKEEQERKEKEEAERKQRG

Table S1. Related to STAR Methods. Amino acid sequences of SAH30 and SAH60 ER/K linkers. The ER/K α-helix sequence derived from *Trichomonas vaginalis* Kelch-motif-containing protein with a helical contour length of 30 nm (top) and the designed sequence with a helical contour length of 60 nm (bottom). The red vertical line indicates the repetition point of fusion of the two SAH30 linkers.

Primer number	Sequence
#1	AAA TCT AGA GCT AGC GGG TCC GGA GTG AGC AAG GGC GAG GAG
#2	AAA AGC GGC CGC AAA GAA TTC CTT GTA CAG CTC GTC CAT
#3	CCC AAG CTT GCG GCC GCC ACC ATG GCC GGC GCC CCC GGC
#4	GCT CAC CAT GGG ATC CTT ATC TCC GGA CCC GCT AGC TCT AGA
#5	TCT AGA GCT AGC GGG TCC GGA GAT AAG GAT CCC ATG GTG AGC
#6	CGG GCC GGG GGC GCC GGC CAT GGT GGC GGC CGC AAG CTT
#7	AGA GCT AGC GGG TCC GGA TAA GCC CCT CTC CCT CCC
#8	CTC GCC CTT GCT CAC CAT TGT GGC CAT ATT ATC ATC
#9	GAT GAT AAT ATG GCC ACA ATG GTG AGC AAG GGC GAG
#10	GGG AGG GAG AGG GGC TTA TCC GGA CCC GCT AGC TCT
#11	CTC ACT ATA GGG AGA CCC AAG CTT ATG GCC GGC GCC CCC GGC CCG CTG
#12	CAG CTC CTC GCC CTT GCT CAC CAT TGT GGC CAT ATT ATC ATC GTG TTT
#13	AAA CAC GAT GAT AAT ATG GCC ACA ATG GTG AGC AAG GGC GAG GAG CTG
#14	CAG CGG GCC GGG GGC GCC GGC CAT AAG CTT GGG TCT CCC TAT AGT GAG
#15	ATA GGG AGA CCC AAG CTT ATG AAG ACC ATC ATC GCC CTG AGC TAC ATC TTC TGC CTG GTG TTC GCC ATG GGG CAA CCC GGG AAC
#16	AAA TCC GGA CCC GCT AGC CAG CAG TGA GTC ATT TGT
#17	CTC ACT ATA GGG AGA CCC AAG CTT ATG AAG ACC ATC ATC GCC CTG AGC
#18	TAG GGG GGG GGG AGG GAG AGG GGC TTA TCC GGA CCC GCT AGC CAG CAG TGA
#19	TCA CTG CTG GCT AGC GGG TCC GGA TAA GCC CCT CTC CCT CCC CCC CCC CTA
#20	GCT CAG GGC GAT GAT GGT CTT CAT AAG CTT GGG TCT CCC TAT AGT GAG

Table S2. Related to STAR Methods. Oligonucleotides used for biosensor construction.

REFERENCES

Agarwal, S.R., Clancy, C.E., and Harvey, R.D. (2016). Mechanisms Restricting Diffusion of Intracellular cAMP. Sci Rep *6*, 19577.

Agarwal, S.R., Yang, P.C., Rice, M., Singer, C.A., Nikolaev, V.O., Lohse, M.J., Clancy, C.E., and Harvey, R.D. (2014). Role of membrane microdomains in compartmentation of cAMP signaling. PLoS One *9*, e95835.

Avet, C., Mancini, A., Breton, B., Le Gouill, C., Hauser, A.S., Normand, C., Kobayashi, H., Gross, F., Hogue, M., Lukasheva, V.*, et al.* (2020). Selectivity Landscape of 100 Therapeutically Relevant GPCR Profiled by an Effector Translocation-Based BRET Platform. bioRxiv, 2020.2004.2020.052027.

Bacskai, B.J., Hochner, B., Mahaut-Smith, M., Adams, S.R., Kaang, B.K., Kandel, E.R., and Tsien, R.Y. (1993). Spatially resolved dynamics of cAMP and protein kinase A subunits in Aplysia sensory neurons. Science *260*, 222-226.

Baillie, G.S. (2009). Compartmentalized signalling: spatial regulation of cAMP by the action of compartmentalized phosphodiesterases. FEBS J *276*, 1790-1799.

Baillie, G.S., Tejeda, G.S., and Kelly, M.P. (2019). Therapeutic targeting of 3',5'-cyclic nucleotide phosphodiesterases: inhibition and beyond. Nat Rev Drug Discov *18*, 770-796.

Bathe-Peters, M., Gmach, P., Boltz, H.H., Einsiedel, J., Gotthardt, M., Hubner, H., Gmeiner, P., Lohse, M.J., and Annibale, P. (2021). Visualization of beta-adrenergic receptor dynamics and differential localization in cardiomyocytes. Proc Natl Acad Sci U S A *118*.

Bathe-Peters M, G.P., Boltz HH, Einsiedel J, Gotthardt M, Hübner H, Gmeiner P, Lohse MJ, Annibale P (2021). Visualization of β-adrenergic receptor dynamics and differential localization in cardiomyocytes. Proc Natl Acad Sci USA *in press*.

Bender, A.T., and Beavo, J.A. (2006). Cyclic nucleotide phosphodiesterases: molecular regulation to clinical use. Pharmacol Rev *58*, 488-520.

Bers, D.M., Xiang, Y.K., and Zaccolo, M. (2019). Whole-Cell cAMP and PKA Activity are Epiphenomena, Nanodomain Signaling Matters. Physiology (Bethesda) *34*, 240-249.

Bock, A., Annibale, P., Konrad, C., Hannawacker, A., Anton, S.E., Maiellaro, I., Zabel, U., Sivaramakrishnan, S., Falcke, M., and Lohse, M.J. (2020). Optical Mapping of cAMP Signaling at the Nanometer Scale. Cell *182*, 1519-1530 e1517.

Borner, S., Schwede, F., Schlipp, A., Berisha, F., Calebiro, D., Lohse, M.J., and Nikolaev, V.O. (2011). FRET measurements of intracellular cAMP concentrations and cAMP analog permeability in intact cells. Nat Protoc *6*, 427-438.

Brunton, L.L., Hayes, J.S., and Mayer, S.E. (1979). Hormonally specific phosphorylation of cardiac troponin I and activation of glycogen phosphorylase. Nature *280*, 78-80.

Buxton, I.L., and Brunton, L.L. (1983). Compartments of cyclic AMP and protein kinase in mammalian cardiomyocytes. J Biol Chem *258*, 10233-10239.

Chen, C., Nakamura, T., and Koutalos, Y. (1999). Cyclic AMP diffusion coefficient in frog olfactory cilia. Biophys J *76*, 2861-2867.

Civciristov, S., Ellisdon, A.M., Suderman, R., Pon, C.K., Evans, B.A., Kleifeld, O., Charlton, S.J., Hlavacek, W.S., Canals, M., and Halls, M.L. (2018). Preassembled GPCR signaling complexes mediate distinct cellular responses to ultralow ligand concentrations. Sci Signal *11*.

Depry, C., Allen, M.D., and Zhang, J. (2011). Visualization of PKA activity in plasma membrane microdomains. Mol Biosyst *7*, 52-58.

Di Benedetto, G., Zoccarato, A., Lissandron, V., Terrin, A., Li, X., Houslay, M.D., Baillie, G.S., and Zaccolo, M. (2008). Protein kinase A type I and type II define distinct intracellular signaling compartments. Circ Res *103*, 836-844.

Drucker, D.J. (2018). Mechanisms of Action and Therapeutic Application of Glucagon-like Peptide-1. Cell Metab *27*, 740-756.

Drucker, D.J., Habener, J.F., and Holst, J.J. (2017). Discovery, characterization, and clinical development of the glucagon-like peptides. J Clin Invest *127*, 4217-4227.

Fischmeister, R., Castro, L.R., Abi-Gerges, A., Rochais, F., Jurevicius, J., Leroy, J., and Vandecasteele, G. (2006). Compartmentation of cyclic nucleotide signaling in the heart: the role of cyclic nucleotide phosphodiesterases. Circ Res *99*, 816-828.

Fletcher, M.M., Halls, M.L., Christopoulos, A., Sexton, P.M., and Wootten, D. (2016). The complexity of signalling mediated by the glucagon-like peptide-1 receptor. Biochem Soc Trans *44*, 582-588.

Fredriksson, R., Lagerstrom, M.C., Lundin, L.G., and Schioth, H.B. (2003). The G-protein-coupled receptors in the human genome form five main families. Phylogenetic analysis, paralogon groups, and fingerprints. Mol Pharmacol *63*, 1256-1272.

Gibson, D.G., Young, L., Chuang, R.Y., Venter, J.C., Hutchison, C.A., 3rd, and Smith, H.O. (2009). Enzymatic assembly of DNA molecules up to several hundred kilobases. Nat Methods *6*, 343-345.

Gold, M.G., Gonen, T., and Scott, J.D. (2013). Local cAMP signaling in disease at a glance. J Cell Sci *126*, 4537-4543.

Halls, M.L., and Cooper, D.M. (2010). Sub-picomolar relaxin signalling by a pre-assembled RXFP1, AKAP79, AC2, beta-arrestin 2, PDE4D3 complex. EMBO J *29*, 2772-2787.

Hauser, A.S., Attwood, M.M., Rask-Andersen, M., Schioth, H.B., and Gloriam, D.E. (2017). Trends in GPCR drug discovery: new agents, targets and indications. Nat Rev Drug Discov *16*, 829-842.

Hayes, J.S., Brunton, L.L., Brown, J.H., Reese, J.B., and Mayer, S.E. (1979). Hormonally specific expression of cardiac protein kinase activity. Proc Natl Acad Sci U S A *76*, 1570-1574.

Hayes, J.S., Brunton, L.L., and Mayer, S.E. (1980). Selective activation of particulate cAMP-dependent protein kinase by isoproterenol and prostaglandin E1. J Biol Chem *255*, 5113-5119.

Houslay, M.D. (2010). Underpinning compartmentalised cAMP signalling through targeted cAMP breakdown. Trends Biochem Sci *35*, 91-100.

Huang, R.C., and Gillette, R. (1993). Co-regulation of cAMP-activated Na+ current by Ca2+ in neurones of the mollusc Pleurobranchaea. J Physiol *462*, 307-320.

Inoue, A., Raimondi, F., Kadji, F.M.N., Singh, G., Kishi, T., Uwamizu, A., Ono, Y., Shinjo, Y., Ishida, S., Arang, N.*, et al.* (2019). Illuminating G-Protein-Coupling Selectivity of GPCRs. Cell *177*, 1933-1947 e1925.

Insel, P.A., Wilderman, A., Zambon, A.C., Snead, A.N., Murray, F., Aroonsakool, N., McDonald, D.S., Zhou, S., McCann, T., Zhang, L.*, et al.* (2015). G Protein-Coupled Receptor (GPCR) Expression in Native Cells: "Novel" endoGPCRs as Physiologic Regulators and Therapeutic Targets. Mol Pharmacol *88*, 181-187.

Koschinski, A., and Zaccolo, M. (2015). A novel approach combining real-time imaging and the patch-clamp technique to calibrate FRET-based reporters for cAMP in their cellular microenvironment. Methods Mol Biol *1294*, 25-40.

Langeberg, L.K., and Scott, J.D. (2015). Signalling scaffolds and local organization of cellular behaviour. Nat Rev Mol Cell Biol *16*, 232-244.

Lefkimmiatis, K., and Zaccolo, M. (2014). cAMP signaling in subcellular compartments. Pharmacol Ther *143*, 295-304.

Lester, L.B., Langeberg, L.K., and Scott, J.D. (1997). Anchoring of protein kinase A facilitates hormone-mediated insulin secretion. Proc Natl Acad Sci U S A *94*, 14942-14947.

Lohse, C., Bock, A., Maiellaro, I., Hannawacker, A., Schad, L.R., Lohse, M.J., and Bauer, W.R. (2017). Experimental and mathematical analysis of cAMP nanodomains. PLoS One *12*, e0174856.

Maiellaro, I., Lohse, M.J., Kittel, R.J., and Calebiro, D. (2016). cAMP Signals in Drosophila Motor Neurons Are Confined to Single Synaptic Boutons. Cell Rep *17*, 1238-1246.

Moller, J., Isbilir, A., Sungkaworn, T., Osberg, B., Karathanasis, C., Sunkara, V., Grushevskyi, E.O., Bock, A., Annibale, P., Heilemann, M.*, et al.* (2020). Single-molecule analysis reveals agonist-specific dimer formation of micro-opioid receptors. Nat Chem Biol *16*, 946-954.

Muller, T.D., Finan, B., Bloom, S.R., D'Alessio, D., Drucker, D.J., Flatt, P.R., Fritsche, A., Gribble, F., Grill, H.J., Habener, J.F.*, et al.* (2019). Glucagon-like peptide 1 (GLP-1). Mol Metab *30*, 72-130.

Nikolaev, V.O., Bunemann, M., Hein, L., Hannawacker, A., and Lohse, M.J. (2004). Novel single chain cAMP sensors for receptor-induced signal propagation. J Biol Chem *279*, 37215-37218.

Nikolaev, V.O., Bunemann, M., Schmitteckert, E., Lohse, M.J., and Engelhardt, S. (2006). Cyclic AMP imaging in adult cardiac myocytes reveals far-reaching beta1-adrenergic but locally confined beta2-adrenergic receptor-mediated signaling. Circ Res *99*, 1084-1091.

Nikolaev, V.O., Moshkov, A., Lyon, A.R., Miragoli, M., Novak, P., Paur, H., Lohse, M.J., Korchev, Y.E., Harding, S.E., and Gorelik, J. (2010). Beta2-adrenergic receptor redistribution in heart failure changes cAMP compartmentation. Science *327*, 1653-1657.

Ovesny, M., Krizek, P., Borkovec, J., Svindrych, Z., and Hagen, G.M. (2014). ThunderSTORM: a comprehensive ImageJ plug-in for PALM and STORM data analysis and super-resolution imaging. Bioinformatics *30*, 2389-2390.

Pandy-Szekeres, G., Munk, C., Tsonkov, T.M., Mordalski, S., Harpsoe, K., Hauser, A.S., Bojarski, A.J., and Gloriam, D.E. (2018). GPCRdb in 2018: adding GPCR structure models and ligands. Nucleic Acids Res *46*, D440-D446.

Rich, T.C., Fagan, K.A., Nakata, H., Schaack, J., Cooper, D.M., and Karpen, J.W. (2000). Cyclic nucleotide-gated channels colocalize with adenylyl cyclase in regions of restricted cAMP diffusion. J Gen Physiol *116*, 147-161.

Rich, T.C., Fagan, K.A., Tse, T.E., Schaack, J., Cooper, D.M., and Karpen, J.W. (2001). A uniform extracellular stimulus triggers distinct cAMP signals in different compartments of a simple cell. Proc Natl Acad Sci U S A *98*, 13049-13054.

Rich, T.C., Xin, W., Mehats, C., Hassell, K.A., Piggott, L.A., Le, X., Karpen, J.W., and Conti, M. (2007). Cellular mechanisms underlying prostaglandin-induced transient cAMP signals near the plasma membrane of HEK-293 cells. Am J Physiol Cell Physiol *292*, C319-331.

Richards, M., Lomas, O., Jalink, K., Ford, K.L., Vaughan-Jones, R.D., Lefkimmiatis, K., and Swietach, P. (2016). Intracellular tortuosity underlies slow cAMP diffusion in adult ventricular myocytes. Cardiovasc Res *110*, 395-407.

Rosenbaum, D.M., Rasmussen, S.G., and Kobilka, B.K. (2009). The structure and function of G-protein-coupled receptors. Nature *459*, 356-363.

Schihada, H., Nemec, K., Lohse, M.J., and Maiellaro, I. (2021). Bioluminescence in G Protein-Coupled Receptors Drug Screening Using Nanoluciferase and Halo-Tag Technology. Methods Mol Biol *2268*, 137-147.

Scott, J.D., and Pawson, T. (2009). Cell signaling in space and time: where proteins come together and when they're apart. Science *326*, 1220-1224.

Sivaramakrishnan, S., and Spudich, J.A. (2011). Systematic control of protein interaction using a modular ER/K alpha-helix linker. Proc Natl Acad Sci U S A *108*, 20467-20472.

Southan, C., Sharman, J.L., Benson, H.E., Faccenda, E., Pawson, A.J., Alexander, S.P., Buneman, O.P., Davenport, A.P., McGrath, J.C., Peters, J.A*., et al.* (2016). The IUPHAR/BPS Guide to PHARMACOLOGY in 2016: towards curated quantitative interactions between 1300 protein targets and 6000 ligands. Nucleic Acids Res *44*, D1054-1068.

Sriram, K., and Insel, P.A. (2018). G Protein-Coupled Receptors as Targets for Approved Drugs: How Many Targets and How Many Drugs? Mol Pharmacol *93*, 251-258.

Stangherlin, A., and Zaccolo, M. (2012). Phosphodiesterases and subcellular compartmentalized cAMP signaling in the cardiovascular system. Am J Physiol Heart Circ Physiol *302*, H379-390.

Sungkaworn, T., Jobin, M.L., Burnecki, K., Weron, A., Lohse, M.J., and Calebiro, D. (2017). Single-molecule imaging reveals receptor-G protein interactions at cell surface hot spots. Nature *550*, 543-547.

Surdo, N.C., Berrera, M., Koschinski, A., Brescia, M., Machado, M.R., Carr, C., Wright, P., Gorelik, J., Morotti, S., Grandi, E*., et al.* (2017). FRET biosensor uncovers cAMP nano-domains at beta-adrenergic targets that dictate precise tuning of cardiac contractility. Nat Commun *8*, 15031.

Taylor, S.S., Ilouz, R., Zhang, P., and Kornev, A.P. (2012). Assembly of allosteric macromolecular switches: lessons from PKA. Nat Rev Mol Cell Biol *13*, 646-658.

Tovey, S.C., Dedos, S.G., Taylor, E.J., Church, J.E., and Taylor, C.W. (2008). Selective coupling of type 6 adenylyl cyclase with type 2 IP3 receptors mediates direct sensitization of IP3 receptors by cAMP. J Cell Biol *183*, 297-311.

Weis, W.I., and Kobilka, B.K. (2018). The Molecular Basis of G Protein-Coupled Receptor Activation. Annu Rev Biochem *87*, 897-919.

Wong, W., and Scott, J.D. (2004). AKAP signalling complexes: focal points in space and time. Nat Rev Mol Cell Biol *5*, 959-970.

Zaccolo, M., Zerio, A., and Lobo, M.J. (2021). Subcellular Organization of the cAMP Signaling Pathway. Pharmacol Rev *73*, 278-309.

Zhang, J.Z., Lu, T.W., Stolerman, L.M., Tenner, B., Yang, J.R., Zhang, J.F., Falcke, M., Rangamani, P., Taylor, S.S., Mehta, S.*, et al.* (2020). Phase Separation of a PKA Regulatory Subunit Controls cAMP Compartmentation and Oncogenic Signaling. Cell *182*, 1531-1544 e1515.

Zhao, P., Liang, Y.L., Belousoff, M.J., Deganutti, G., Fletcher, M.M., Willard, F.S., Bell, M.G., Christe, M.E., Sloop, K.W., Inoue, A.*, et al.* (2020). Activation of the GLP-1 receptor by a non-peptidic agonist. Nature *577*, 432-436.